# Profiling the Non-genetic Origins of Cancer Drug Resistance with a Single-Cell Functional Genomics Approach Using Predictive Cell Dynamics

Mickael Meyer, Agnès Paquet, Marie-Jeanne Arguel, Ludovic Peyre, Luis Gomes-Pereira, Kevin Lebrigand, Baharia Mograbi, Patrick Brest, Rainer Waldmann, Pascal Barbry, et al.

Cell Systems



# Profiling the Non-genetic Origins of Cancer Drug Resistance with a Single-Cell Functional Genomics Approach Using Predictive Cell Dynamics

## Graphical Abstract

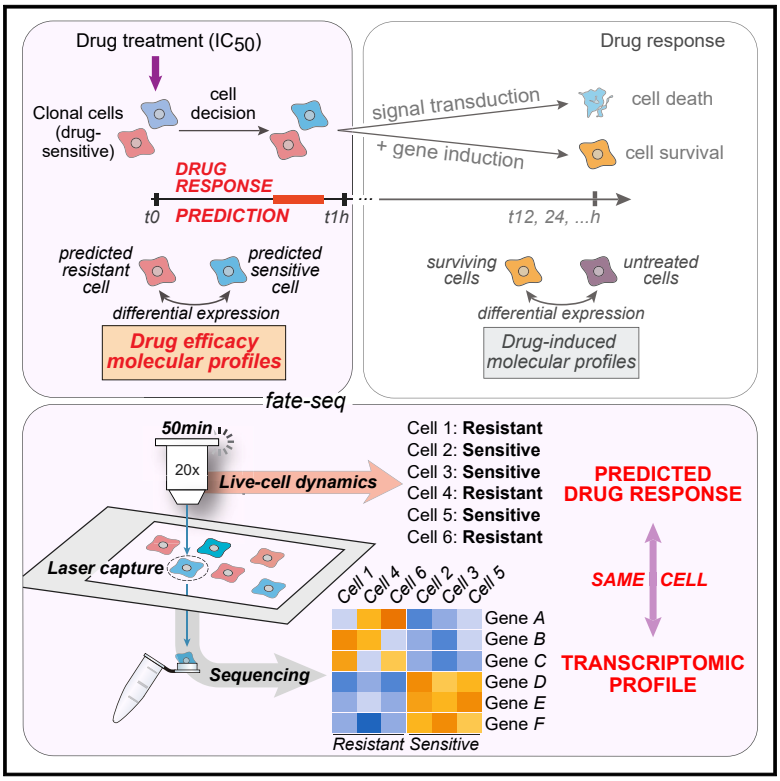


## Highlights

- Fate-seq links the drug response of a single cell to its own transcriptomic profile
- Fate-seq recovers variable cell decision information from unstructured variability
- It identifies molecular factors causing the intrinsic resistance to cancer drugs
- A TRAIL therapeutic efficacy profile is performed in HeLa cells as proof of concept

## Authors

Mickael Meyer, Agnès Paquet, Marie-Jeanne Arguel, ..., Pascal Barbry, Paul Hofman, Jérémie Roux

## Correspondence

jeremie.roux@univ-cotedazur.fr

## In Brief

For most cancer drug treatments, a fraction of the clonal cell population can survive because of non-genetic cell-to-cell variability. We present fate-seq, a method to determine the molecular origins of this heterogeneous drug response, by comparing the transcriptomic profiles of predicted resistant versus predicted sensitive cells, before treatment induces confounding changes.

Meyer et al., 2020, Cell Systems *11*, 1–8
October 21, 2020 
https://doi.org/10.1016/j.cels.2020.08.019

CellPress

Please cite this article in press as: Meyer et al., Profiling the Non-genetic Origins of Cancer Drug Resistance with a Single-Cell Functional Genomics Approach Using Predictive Cell Dynamics, Cell Systems (2020), https://doi.org/10.1016/j.cels.2020.08.019

Cell Systems

CellPress
OPEN ACCESS

Methods in Brief

# Profiling the Non-genetic Origins of Cancer Drug Resistance with a Single-Cell Functional Genomics Approach Using Predictive Cell Dynamics

Mickael Meyer,[1,4] Agnès Paquet,[2,4] Marie-Jeanne Arguel,[2] Ludovic Peyre,[1] Luis C. Gomes-Pereira,[3] Kevin Lebrigand,[2] Baharia Mograbi,[1] Patrick Brest,[1] Rainer Waldmann,[2] Pascal Barbry,[2] Paul Hofman,[1] and Jérémie Roux[1,5,*]

[1]Université Côte d'Azur, CNRS UMR 7284, Inserm U 1081, Institut de Recherche sur le Cancer et le Vieillissement de Nice, Centre Antoine Lacassagne, 06107 Nice, France

[2]Université Côte d'Azur, CNRS UMR 7275, Institut de Pharmacologie Moléculaire et Cellulaire, Sophia Antipolis, 06560 Nice, France

[3]Université Côte d'Azur, Inria, INRAE, CNRS, Sorbonne Université, Biocore team, Sophia Antipolis, 06560 Nice, France

[4]These authors contributed equally

[5]Lead Contact

*Correspondence: jeremie.roux@univ-cotedazur.fr

https://doi.org/10.1016/j.cels.2020.08.019

## SUMMARY

Non-genetic heterogeneity observed in clonal cell populations is an immediate cause of drug resistance that remains challenging to profile because of its transient nature. Here, we coupled three single-cell technologies to link the predicted drug response of a cell to its own genome-wide transcriptomic profile. As a proof of principle, we analyzed the response to tumor-necrosis-factor-related apoptosis-inducing ligand (TRAIL) in HeLa cells to demonstrate that cell dynamics can discriminate the transient transcriptional states at the origin of cell decisions such as sensitivity and resistance. Our same-cell approach, named fate-seq, can reveal the molecular factors regulating the efficacy of a drug in clonal cells, providing therapeutic targets of non-genetic drug resistance otherwise confounded in gene expression noise. A record of this paper's transparent peer review process is included in the Supplemental Information.

## INTRODUCTION

Isogenic cell populations exhibit multiple scales of non-genetic heterogeneity, from gene expression to phenotypic response. Clonal cells in the same phenomenological state, such as cell cycle or differentiation stages, can still respond differently to the same stimulus (Purvis et al., 2012; Spencer et al., 2009). A common hypothesis for this cell-to-cell phenotypic heterogeneity is the co-existence, within isogenic cell populations, of different cellular states that arise from stochasticity in the biochemical reactions controlling molecules biosynthesis and degradation (Balázsi et al., 2011; Elowitz et al., 2002; Loewer et al., 2013; Raj and van Oudenaarden, 2008). These processes generate biological noise that can facilitate cell decisions such as growth, adaptation, cell proliferation, differentiation, and drug response, in a non-genetic fashion, yet constant and apparently regulated (Albeck et al., 2013; Mitchell et al., 2018; Purvis et al., 2012; Saint et al., 2019; Santos et al., 2007; Spencer et al., 2009; Süel et al., 2006).

In addition, non-genetic heterogeneity has also been linked to tumor formation—cell evading apoptosis—and incomplete eradication of tumor clones (Marusyk et al., 2012; Reyes and Lahav, 2018). Recent studies including ours have shown that the incomplete response to cancer therapeutics (fractional killing) is due to differences in cell response dynamics (Paek et al., 2016; Roux et al., 2015). Heterogeneous cell signaling dynamics play a significant role in the efficacies of many cancer drugs where most of the "sensitive cell lines" still respond partially at the population level, with only a fraction of cells undergoing apoptosis at saturating doses (Fallahi-Sichani et al., 2013; Forcina et al., 2017). Even after repeated rounds of drug challenges, drug-tolerant persister cells have been shown to mediate this fractional killing, suggesting that the same individual cell can switch between opposing phenotypic responses (Flusberg et al., 2013; Sharma et al., 2010; Su et al., 2017). Phenotypic switching, a survival strategy without *de novo* mutation (Acar et al., 2008), is a form of drug evasion that has been shown to lead to genetic drug resistance, ultimately accounting for cancer therapeutic failure (Ramirez et al., 2016; Shaffer et al., 2017; Sharma et al., 2010). Thus, understanding the molecular basis of this drug response phenotype switching at the single-cell level has implications for cancer therapeutic development (Salgia and Kulkarni, 2018). Death receptor agonists, such as tumor-necrosis-factor-related apoptosis-inducing ligand (TRAIL), are excellent models for studying the origins of drug response heterogeneity, as they were proven disappointing in clinical trials due to fractional killing, evidenced by a low maximum drug effect ($E_{max}$) (Gonzalvez and Ashkenazi, 2010; Holland, 2014). However, identifying the molecular determinants of drug response heterogeneity has been impaired by the technical and analytical

Please cite this article in press as: Meyer et al., Profiling the Non-genetic Origins of Cancer Drug Resistance with a Single-Cell Functional Genomics Approach Using Predictive Cell Dynamics, Cell Systems (2020), https://doi.org/10.1016/j.cels.2020.08.019



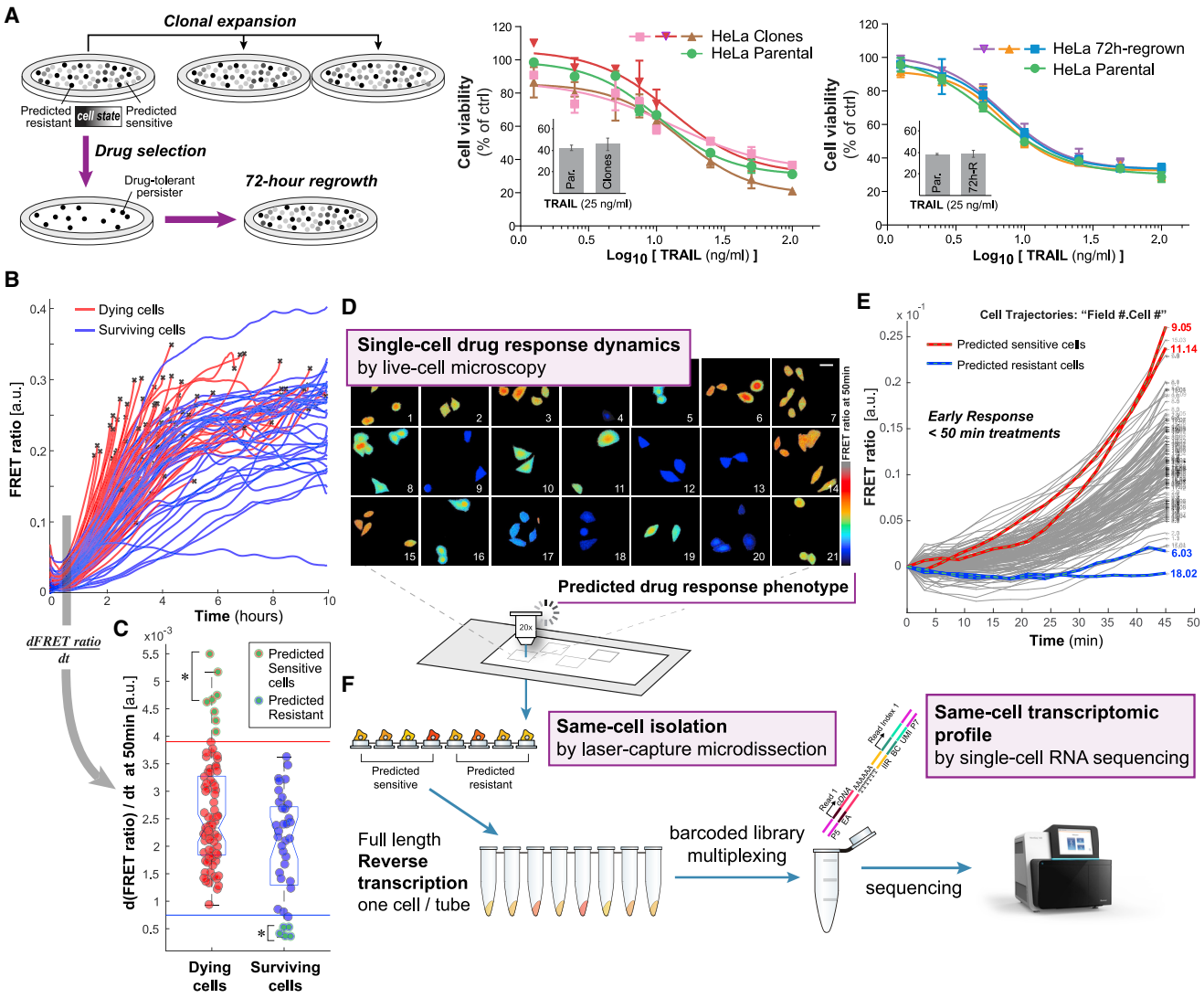


**Figure 1. Constant Proportioning of Cell Response Heterogeneity Enables Stable Predictive Metrics of Drug Response for Phenotype-Coupled Same-Cell Profiling: Fate-Seq**

(A) Clonal expansion and drug selection reveal the plasticity of drug response phenotypes in isogenic cells. For clonal expansion: single-cell clones were obtained by limiting dilutions of the HeLa parental cells. For drug selection: parental HeLa cells were treated with TRAIL (25 ng/mL for 15 h). The surviving cells from the first treatments were allowed to regrow for 72 h. Once the surviving cells and the sub-clones had regrown into new cultures (72 h and 3 weeks, respectively), they were all treated with TRAIL at several doses, and their responses were compared with the parental cells. One representative dose response profile is shown for both clonal expansion and drug selection experiments. Bar graphs represent cell viability from at least three biological repeats of both clonal expansion and drug selection experiments. Cell viability was assessed 15 h post-treatment by CellTiter-Glo, and the absorbance is represented in percent of control relative to cell population treated with TRAIL-vehicle, data are represented as mean ± SD.

(B) Single-cell trajectories of FRET ratio reporting caspase-8 activity. Live-cell microscopy experiments (> 10 h) were performed to establish the caspase-8 dynamics predicting the ultimate cell fate after treatment with TRAIL (25 ng/mL in HeLa cells stably expressing the FRET biosensor IC-RP; Albeck et al., 2008). One representative experiment of 143 tracked cells is presented.

(C) The caspase-8 activation rate (time derivative of FRET ratio, dFRET ratio/dt; Roux et al., 2015) after TRAIL stimulation is calculated of for each single cell: we found a time after treatment (50 min) at which caspase-8 activation rate could accurately predict the ultimate cell response at the end of the experiment, using constant thresholds (colored lines; measured in at least three experiments). The star indicates the top 4 predicted cells of each group that can be processed in fate-seq (Figure 2). The cell fate prediction being done after 50-min TRAIL stimulation limits gene induction (Figure S1B) and allows to isolate the sensitive cells that would otherwise die.

(D) Example live-cell microscopy experiment for caspase-8 early activation measurement in each identified cell. 50-min live-cell microscopy experiment was performed to collect caspase-8 dynamics for each cell cultured on a membrane ready for micro-dissection. About 20 fields of cells are monitored, and all cells are tracked for their FRET signal in time.

(E) Single-cell trajectories of FRET ratio are reported for each cell tracked to perform the fate prediction based on their caspase-8 activation rate (dFRET ratio/dt) 50-min post-TRAIL treatment (25 ng/mL, see Figure 1C). One representative experiment of 158 tracked cells is presented. Red and blue trajectories with green dash lines were predicted sensitive and predicted resistant cells, respectively. Note that a single measure of the FRET ratio at 50 min would not be sufficient to

*(legend continued on next page)*

Please cite this article in press as: Meyer et al., Profiling the Non-genetic Origins of Cancer Drug Resistance with a Single-Cell Functional Genomics Approach Using Predictive Cell Dynamics, Cell Systems (2020), https://doi.org/10.1016/j.cels.2020.08.019



impediments of multimodal single-cell approaches. Indeed, measuring signaling dynamics or phenotypic response and global gene expression profiles in the same cell has been technically challenging, not to mention that drug treatment itself either deteriorates the integrity of sensitive cells or induces an associated genomic response. Targeted CRISPR screens (Adamson et al., 2016; Datlinger et al., 2017; Dixit et al., 2016; Jaitin et al., 2014; Rubin et al., 2019) have opened up opportunities to same-cell studies with the caveat that each factor chosen to be targeted has its own cell line that will differ from the parental cells prior the phenotype assessment (limiting the molecular targets examined and subjecting the measured cells to some of the biases of genetic reprogramming). As a consequence, the relationship between global -omic signatures and phenotypic measures has stayed mainly correlative.

To overcome these limitations, we designed a workflow coupling three single-cell technologies: we used a predictive measure of single-cell response by live-cell microscopy, in order to isolate predicted sensitive and predicted resistant cells by laser-capture microdissection and then profiled each captured cell by single-cell RNA sequencing directly (with no cell dissociation, sorting, nor microfluidics handling). This allowed to determine in the same cell, the genome-wide transcriptomic profile at the mechanistic origin of cellular drug response and establish as a proof of principle, a single-cell functional signature of TRAIL therapeutic efficacy.

## RESULTS

### Single Cells Perpetuate Population Heterogeneity in Constant Proportions, Providing Features for Cell Fate Prediction

Phenotypic switching, which implies unstable phenotypes at the level of each single cell, makes it difficult to associate cell profiles to their future drug response phenotypes. To first evaluate the stability (interconversion property) of the two drug response phenotypes observed within a clonal HeLa cell population treated with TRAIL (cell death or survival), we performed several rounds of clonal expansion and drug selection. HeLa cells were either sub-cloned into new cultures or treated with TRAIL at around their $IC_{50}$ (25 ng/mL) to put the non-responding cells into new cultures. We found that cells derived from clonal expansion or drug selection of parental HeLa cells could produce new cell populations of similar and constant drug response profiles, regardless of the cell clone or their response phenotype to the first drug treatment (Figure 1A). Although this observed non-genetic resistance is transient, with cells switching phenotypes, we found that each cell could perpetuate the drug response heterogeneity of the population, in constant proportions.

While the potential fate of a cell is unstable, we had previously shown that it is correlated with the initiator caspase (caspase-8) maximal activity during the course of TRAIL treatment (Roux et al., 2015). (However, the maximal caspase-8 activity is reached at cell death for the sensitive cells, which had defied its use as a predictive measure to assess cell fate upon treatment.) With the proportioning of the cell responses being constant at the population level, we sought to evaluate in each cell, the caspase-8 activation rate systematically after drug addition and associate it with the cell response phenotype at the end of the experiment (dying or surviving cell). By doing so, we found that caspase-8 activation rate at 50 min post-treatment was a robust predictor of cell fate for the most differing cells (Figures 1B and 1C). We, thus, could define two thresholds (sensitive and resistant) that were constant between training experiments and with which the prediction could accurately classify the response phenotype of the cells (Figure 1C), at a time after TRAIL treatment where no significant change was induced at the transcriptomic level (Figure S1), and no cell had yet executed cell death.

Although there was no transcriptomic change detectable after a short TRAIL treatment, we sought to verify whether some gene expression variability between the 50-min TRAIL-treated cells could indicate their response phenotypes. We analyzed 3,000 single cells—resting and 50-min TRAIL-treated cells, using the 10X platform (10X Genomics B.V., the Netherlands): after regressing out the cell-cycle component, we could not identify pre-existing cell-to-cell differences in genes of the TRAIL-signaling pathway that would recapitulate the constant fractional response (Figures S1A–S1D). Although isogenic populations contain cells in different states (such as the different phases of the cell cycle), classic single-cell RNA sequencing could not discriminate drug-sensitivity or -resistance states, because of the lack of known gene markers to identify these clusters.

Together, these experiments showed that although the response of a cell may switch between resistant and sensitive, there is no emerging feature in their global transcriptomic state that can help detecting these different cell states. However, we show here that early caspase-8 activation rates can predict the ultimate cell response of the most differing cells, which could be used to enrich these rare cell groups prior to sequencing and establish the markers of drug efficacy.

### Single-Cell Response Prediction Coupled to Same-Cell Isolation *In Situ*

The measured gene expression variability of isogenic cells has been so far referred to as gene expression noise (unstructured variability; Eling et al., 2019) instead of an observable signal, in part because of the lack of prior knowledge on the different states of a cell, such as the drug-sensitivity states. To address this issue, we designed a same-cell functional pharmacogenomics approach that couples the prior knowledge of the cell phenotypic state (predicted cell fate) to the transcriptomic profile of the same cell: fate-seq (Figures 1D–1F). Predicted cell fate is determined with the response dynamic profile of each cell monitored by live-cell microscopy: in each experiment ~150 cells were imaged and tracked for 50 min post-TRAIL treatment to perform cell fate predictions. Cells that showed a definitive commitment based on their caspase-8 activation rate (as cells

determine the cell fate, as the basal activity ratio differs between untreated cells (normalization to the same cell at time 0 must be done), and because the predictive metric is based on the time derivative of the FRET ratio, which requires two consecutive measures of the same cell in time.

(F) Each cell has been tracked so to allow the same cell to be phenotyped in live-cell microscopy, isolated by laser-capture microdissection and profiled by single-cell RNA-seq. Two to 8 single-cells were captured and sequenced per fate-seq experiment.

Please cite this article in press as: Meyer et al., Profiling the Non-genetic Origins of Cancer Drug Resistance with a Single-Cell Functional Genomics Approach Using Predictive Cell Dynamics, Cell Systems (2020), https://doi.org/10.1016/j.cels.2020.08.019



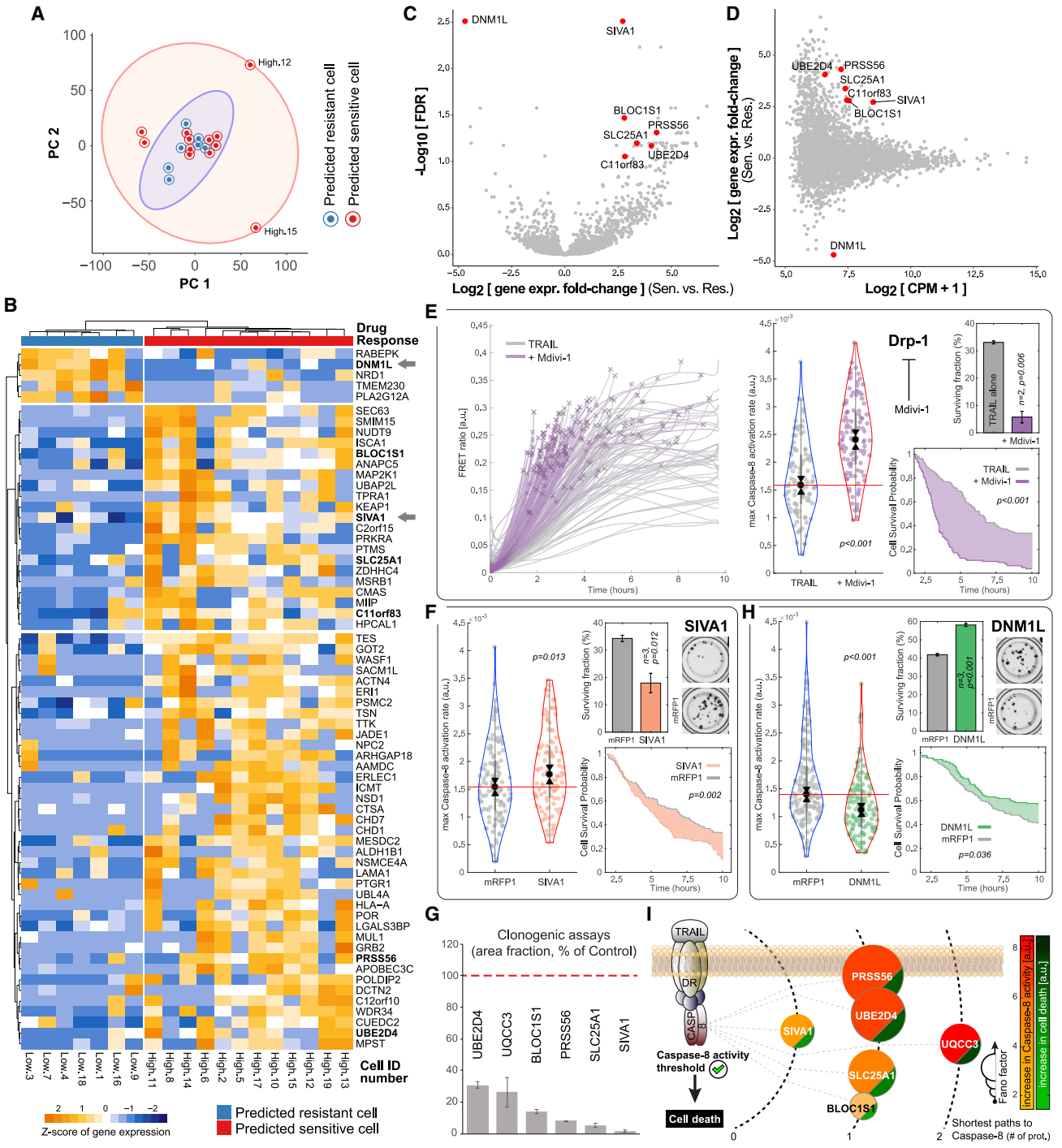


**Figure 2. Fate-Seq Recovers a Drug-Efficacy Gene Signature from Unstructured Variability: Profiling TRAIL Response as a Proof of Principle**

Cells selected based on their predicted phenotype 50-min post-TRAIL treatment (25 ng/mL) were assayed by single-cell RNA sequencing.

(A) Principal component analysis of the single-cell RNA-seq. Each dot represents a cell colored by its predicted phenotype. "High" refer to cells in (B).

(B) TRAIL sensitivity signature of HeLa cells: hierarchical clustering of genes (FDR < 0.1 and $|\log_2(FC)| > 2$) from selected cells highlights the heterogeneity of cancer drug response information contained in isogenic cells treated together. "High" and "low" refer to the cell identifier in dataset.

(C) *Volcano-plot*: x axis represents the difference in average gene expression between predicted sensitive and predicted resistant cells ($\log_2$ scale). y axis represents the FDR ($-\log_{10}$ FDR). Red dots represent the gene candidates for functional validations.

(D) *MA-plot*: x axis represents the average gene expression for each gene ($\log_2$ CPM + 1). y axis represents the difference in gene expression between predicted sensitive (high) versus predicted resistant cells (low), $\log_2$ scale. Red dots represent the gene candidates for functional validations.

*(legend continued on next page)*

Please cite this article in press as: Meyer et al., Profiling the Non-genetic Origins of Cancer Drug Resistance with a Single-Cell Functional Genomics Approach Using Predictive Cell Dynamics, Cell Systems (2020), https://doi.org/10.1016/j.cels.2020.08.019



in starred-brackets Figure 1C) were captured by laser microdissection. With this, the predicted sensitive and predicted resistant cells that had been cultured in population could be directly isolated *in situ* without dissociation, immediately lysed and processed individually (one cell per tube). Barcoded cells from several experiments were then pooled for multiplexed single-cell RNA sequencing (Figure S2; QC metrics in Table S1). Since lost cells, debris, or captured doublets could not be checked by visual inspection once catapulted in the tube, stringent exclusion criteria were used after sequencing, based on UMI counts and dropout rates, supplying 19 cells for further analysis (from 54 cells collected in 8 experiments).

The devised predictive measure is of particular interest because (1) it allows to determine accurately the response phenotype of a cell before drug stimulation could induce major confounding changes in its transcriptomic profile (as shown in Figure S1B) and because (2) it allows to recover both resistant and sensitive cells, while other analyses can only compare resistant cells to an untreated sample. By coupling the prediction of a cell response to transcriptomic profiling of the same cell, fate-seq should provide a link between a cell molecular state and its resulting phenotype, with cell signatures of drug efficacy.

## Fate-Seq Reveals a Drug Sensitivity Signature within Gene Expression Variability

We first validated by principal component analysis and unsupervised hierarchical clustering that predicted sensitive and resistant cells to TRAIL did not cluster in separate regions of the first two principal components landscape (Figure 2A) and that the clustering was not linked to the presence of confounding factors such as batches of single-cell collections, cell-cycle phase prediction, or even predicted phenotype (Figure S3A). These results confirmed that although the cell fate decision was already determined for these cells, their potential expression difference was still confounded within gene expression noise when compared classically. A hierarchical clustering analysis based on the genes with the most significant biological variation, highly variable genes (Lun et al., 2016), could not recover the two predicted cell response phenotypes either (Figure S3B).

However, by grouping cells based on their predicted response phenotype, pathway enrichment analyses significantly ranked functions such as "cell death and survival" (Figure S4), indicating that we had increased the meaningful expression signal by performing differential expression analysis between our predicted cell groups. Hierarchical clustering based on the most significant differentially expressed genes (false discovery rate [FDR] < 0.1 and $|\log_2(FC)| > 2$) highlighted the heterogeneity of anticancer drug sensitivity information contained in identical cells treated together and revealed the TRAIL-efficacy gene signature in HeLa cells (Figure 2B; arrows point to the top gene target of each response category. Differential expression analyses results provided in Table S2). We then derived a short list of target genes intersecting on a couple of statistical criteria (minimal FDR, minimal dropout rate, maximal fold change with sufficiently high expression levels in both predicted phenotypic responses, Figures 2C and 2D): top target genes *DNM1L* and *SIVA1* as well as *BLOC1S1*, *PRSS56*, *SLC25A1*, *UBE2D4*, and *C11orf83* (named *UQCC3* hereafter).

To initiate the functional validation of the target genes, we first used inhibitor drugs for a protein whose gene was highly expressed in predicted resistant cells. Targeting dynamin-1-like protein (DRP1), encoded by *DNM1L* (top gene target found highly expressed in resistant cells, Figures 2C and 2D), we found that both mdivi-1 and dynasore (DRP1 and dynamins inhibitors, respectively) could significantly increase TRAIL-induced caspase-8 activity (Figures 2E and S5). In addition, these treatment combinations with mdivi-1 or dynasore, consequently increased cell death response compared with TRAIL alone: shortening by

(E) Pharmacological validations of top target gene *DNM1L* using co-treatment with inhibitor drugs. Live-cell microscopy experiments evaluating the effect of Mdivi-1 (25 μM) in combination or not with TRAIL treatment (25 ng/mL) in parental cells expressing IC-RP only. FRET ratio trajectories: 266 cells were tracked in the 10-h representative experiment shown (controls shown in Figures S5E and S5F). Violin plots: maximal caspase-8 activation rate of each cell for each condition of the same representative experiment. Survival curves: cell death times of each condition in the representative experiment (event determined by morphology assessment in live-cell microscopy). Bar graphs: average cell surviving fraction at the end of the live-cell microscopy experiments (10 h, dead cell counts determined by morphology assessment) for 2 experimental repeats (547 cells were tracked in total), data are represented as mean ± SEM.

(F) Functional validations of top differentially expressed gene *SIVA1*, using engineered cell lines: single-cell assessments of caspase-8 activation and cell survival upon treatment with TRAIL (25 ng/mL) performed by live-cell microscopy experiments evaluating the effect of overexpressing the target gene in parental HeLa cells expressing IC-RP. Control cells (mRFP1) are IC-RP parentals, overexpressing mRFP1 fluorescent protein only. Violin plots: maximal caspase-8 activation rate of each cell for each condition of one representative experiment where 276 cells were tracked. Survival curves: cell death times of each condition in the same representative experiment (event determined by morphology assessment in live-cell microscopy). Bar graphs: average cell surviving fraction at the end of the live-cell microscopy experiments (10 h, dead cell counts determined by morphology assessment) for 3 experimental repeats (831 cells were tracked in total), data are represented as mean ± SEM. Clonogenic assays: one representative experiment of at least 3 experimental repeats of crystal-violet stained cells in 96-well plates, 1 week after a 24-h treatment with TRAIL (250 ng/mL).

(G) Average clone area fraction from at least three clonogenic assays for each cell line overexpressing a short-listed target gene *UBE2D4*, *UQCC3* (*c11orf83*), *BLOC1S1*, *PRSS56*, *SLC25A1*, and *SIVA1* compared with IC-RP parentals overexpressing mRFP1 fluorescent protein only. Crystal-violet stained cells in 96-well plates, 1 week after a 24-h treatment with TRAIL (250 ng/mL), were photographed, and the well area fraction occupied by cell colonies was evaluated in ImageJ, data are represented as mean ± SD.

(H) Functional validations of top differentially expressed gene *DNM1L*, performed by live-cell microscopy experiments as described in (F) above. Violin plots: maximal caspase-8 activation rate of each cell for each condition of one representative experiment where 349 cells were tracked. Survival curves: cell death times of each condition in the same representative experiment (event determined by morphology assessment in live-cell microscopy). Bar graphs: average cell surviving fraction at the end of the live-cell microscopy experiments (10 h, dead cell counts determined by morphology assessment) for 3 experimental repeats (1,017 cells were tracked in total), data are represented as mean ± SEM. Clonogenic assays: same as in (F).

(I) Diagram of the shortest paths between the target genes that increase cell death and caspase-8 on concentric half-circles with dashed lines (DR, death receptors; CASP8, caspase-8). For each gene of the TRAIL efficacy signature established in HeLa cells, the size of the colored circle is proportional to its Fano factor (variance/mean expression ratio of each gene), and the color gradients are scaled on its relative effect on caspase-8 activity and on cell death. The caspase-8 activity threshold (Roux et al., 2015, direct relationship between caspase-8 activation and cell death) is preserved for each gene.

Please cite this article in press as: Meyer et al., Profiling the Non-genetic Origins of Cancer Drug Resistance with a Single-Cell Functional Genomics Approach Using Predictive Cell Dynamics, Cell Systems (2020), https://doi.org/10.1016/j.cels.2020.08.019



2.2-fold the half-life of the cell population and decreasing cell survival probability below 0.1 (versus 0.32 in control cells, Figures 2E and S5). A translation inhibitor and an inhibitor for targets further down the list of differentially expressed genes were used as positive and negative controls respectively (Figures S6 and S7, respectively).

We then engineered cell lines to overexpress the shortlisted genes that were found highly expressed in predicted sensitive cells: top target gene *SIVA1* as well as *BLOC1S1*, *PRSS56*, *SLC25A1*, *UBE2D4*, and *UQCC3* (*c11orf83*), all in fusion with the fluorescent protein mRFP1. Using live-cell microscopy, we compared each cell line to control cells (established in parallel but overexpressing mRFP1 only) by monitoring their caspase-8 activation and survival rates after TRAIL treatment; an average of 850 cells were tracked per gene validation. We also measured by clonogenic assays, the capacity of drug-tolerant persisters to produce cell colonies after TRAIL treatment. We found that overexpression of *SIVA1*, *PRSS56*, *SLC25A1*, *UBE2D4*, and *UQCC3*, all increased significantly the rate of caspase-8 activation induced by TRAIL (Figures 2F and S8A, these observations confirmed the validity of the screening criteria). Cell sensitivity to TRAIL was correspondingly increased in engineered cell lines with these target genes. In addition, we could also validate a long-term effect of these gene perturbations, by showing that all target genes could significantly reduce the number of colonies produced by drug-tolerant persisters after a treatment with TRAIL (Figures 2F and S8A, all quantifications in Figure 2G). Overexpression of *SIVA1* could also increase cell sensitivity to death receptor therapeutic antibodies such mapatumumab ($IC_{50}$ = 0.148 nM versus 0.373 nM in parental cells) and drozitumab ($IC_{50}$ = 75.4 versus 123.5 ng/mL in parental cells, with anti-Fc antibody cross-linking). Conversely, as expected, overexpression of *DNM1L* significantly decreased caspase-8 activation rate, cell sensitivity to TRAIL and increased the number of colonies from drug-tolerant persisters (Figure 2H), further validating the approach. A gene that was further down the list of differentially expressed genes with no statistically significant difference, *LLPH*, was used as overexpression control (Figure S8C).

Together these results showed that our same-cell functional pharmacogenomics approach allowed the identification of a set of target genes that could both predict and perturb the non-genetic drug resistance to TRAIL, constituting a drug efficacy gene signature that differ from drug-induced gene signatures.

## DISCUSSION

It is now possible with the approach described here to recover cell decision information from unstructured variability in gene expression (i.e., biological noise) by monitoring the same cell across the screening from phenotype prediction to single-cell transcriptomics. We demonstrated that this approach reveals the transcriptomic profiles at the mechanistic origin of cell response, as opposed to the therapy-induced profile in resistant cells. As a proof of principle, we used this method to uncover a cell sensitivity signature to TRAIL, composed of factors regulating the population response proportioning that gives rise to drug resistance within a clonal cell population. This set of genes, *DNM1L*, *SIVA1*, *BLOC1S1*, *PRSS56*, *SLC25A1*, *UBE2D4*, and *UQCC3*, could be specifically perturbed to increase cell sensitivity to death receptor agonists. These genes were found to participate to the fast phenotypic switching between resistant and sensitive cell states, due to the natural gene expression heterogeneity of an isogenic cell population. Clonogenic assays ultimately confirmed that stabilizing the expression of the identified target genes could rescue cell sensitivity to the drug with long-term benefits. These results, therefore, suggest that the method presented here can identify sets of biomarker candidates as well as co-drugs improving the pharmacological profiles of primary treatments that lack efficacies because of cell-to-cell variability within a cell type or clone. We also observed that the amount of expression variability of a target gene seemed correlated to its rescue capacity. Indeed, by evaluating the shortest path between the target genes and caspase-8, we found that at equal distance, the noisier (highest Fano factor) the expression in parental cells was the larger the effect a gene overexpression had on caspase-8 activity and ultimately, cell death (Figure 2I, at similar variability: the longer the shortest path, the larger the effect). These observations also support the hypothesis that signaling networks utilize noise to increase population-level information transfer and regulate the overall cell population response (Suderman et al., 2017). With the shortlisted target genes validated to affect the drug response, our results suggest that same-cell functional pharmacogenomics screens, comparing isogenic cells treated together, are promising methods to reveal regulatory factors and therapeutic targets of non-genetic drug resistance, providing a substrate for developing the tools of rationale combination therapy in systems pharmacology.

Since transient non-genetic resistance is not stably inherited in sister cells (as opposed to epigenetic phenotypes [Dawson, 2017]), classic single-cell multimodal analyses of induced or inherited factors (Bell et al., 2019; Kim et al., 2018) remained inappropriate to study the molecular determinant of transient resistance, where each single-cell can give rise to an equally heterogeneous cell population, invariably exhibiting the same drug response heterogeneity. With our approach, however, we started to address the long-standing question on how heterogeneous cell states can inform cell decision, by applying the method to cancer drugs transient resistance. Indeed, the question whether a cell can evade cancer treatment thanks to preexisting cellular state differences, remains unanswered owing to a fundamental limitation: the latency of the cell fate decision (the cell decision is only observable at the time when sensitive cells disappear and resistant cells emerge with an induced-genomic profile). A key aspect here is to use predictions of drug response in order to preserve all cells in the population; this allowed the analyses of responding versus non-responding cells within the same drug-sensitive population at a nearly naive transcriptional state. By studying single cells together, comparing cell response within the same population and acquiring both the response prediction with the transcriptomic profile of the same cell, our approach reveals cell decision information otherwise confounded by gene expression noise within or between cell samples.

As clinical assessment of sub-clonal heterogeneity becomes a relevant information during cancer diagnosis (Karaayvaz et al., 2018), the cellular mechanisms that regulate the cell states within a tumor clone (drug responding and non-responding states) will be critical for cancer drug development. Here, we propose a multimodal profiling methodology to pair a non-destructive

measurement, such as a pharmacological profile, to single-cell RNA sequencing. Unlike other single-cell multimodal profiling methods using microfluidics (Lane et al., 2017) or fluorescent-activated cell sorting (FACS, the most widely used solution; Stuart and Satija, 2019), our approach allows repeated measurements of the same cell in population and *in situ* to gather predictive drug response dynamics before the destructive assay. The framework, therefore, enables the identification of molecular factors causing in the incomplete response of sensitive cell types to cancer therapeutics (rather than induced factors). With the field of dynamic biomarkers growing rapidly (Liu et al., 2019), this framework is amenable to all multi-omics methods to isolate single cell based on their drug response profile and reveal sets of biomarkers or networks of molecular factors that can readily be targeted to improve the pharmacological profiles of primary treatments impaired by cellular heterogeneity.

## STAR★METHODS

Detailed methods are provided in the online version of this paper and include the following:

- KEY RESOURCES TABLE
- RESOURCE AVAILABILITY
  - Lead Contact
  - Materials Availability
  - Data and Code Availability
- EXPERIMENTAL MODEL
- METHOD DETAILS
  - Plasmids and Cloning
  - Cell Line Constructions
  - Quantitative PCR
  - Cell Viability
  - Clonogenic Assays
  - Live-Cell Microscopy
  - Laser-Capture Microdissection
  - Laser-Captured Single-Cell Sequencing
  - Droplet-based Single-Cell Sequencing
- QUANTIFICATION AND STATISTICAL ANALYSIS
  - Live-Cell Imaging Analyses
  - Laser-Captured Single-Cell Analyses
  - Statistical Analyses
  - Droplet-based Single-Cell Analyses

## SUPPLEMENTAL INFORMATION

Supplemental Information can be found online at https://doi.org/10.1016/j.cels.2020.08.019.

## ACKNOWLEDGMENTS

We thank Virginie Magnone and Laure-Emmanuelle Zaragosi for help with the 10x Genomics experiments, Nadir Djerbi for the live-cell microscopy setup at the IRCAN's Molecular and Cellular Core Imaging (PICMI) Facility (supported by funding from FEDER, Conseil Régional Provence-Alpes-Côte d'Azur, Conseil Départemental 06, Cancéropôle PACA, Gis Ibisa et Inserm), as well as Maeva Gesson and Damien Alcor for the laser microdissection setup at Centre Méditerranéen de Médecine Moléculaire (C3M/INSERM 1065). Single-cell RNA sequencing was performed by UCAGenomiX, a partner platform of the National Infrastructure France Génomique (ANR-10-INBS-09-03 and ANR-10-INBS-09-02), with support from Conseil Départemental des Alpes Maritimes (2016-358 294DGADSH-CV) and Canceropôle PACA. This work was funded by a Marie Curie International Incoming Fellowship within the 7th European Community Framework Programme (proposal SysBioDRez, no. 626190, call reference: FP7- PEOPLE-2013-IIF), an INCa Plan Cancer Biologie Des Systèmes, ITMO Cancer (proposal IMoDRez, no.18CB001-00), a young investigator award (Emergence Jeunes Chercheurs), as well as a Single-cell Starting package from Canceropôle Provence-Alpes-Côte d'Azur, the French National Cancer Institute (INCa), and the Provence-Alpes-Côte d'Azur Region, to J.R.

## AUTHOR CONTRIBUTIONS

Investigation, M.M., M.-J.A., L.P., R.W., and J.R.; Formal Analysis, A.P., L.C.G.-P., K.L., and J.R.; Data Curation, K.L. and A.P.; Resources, B.M., P. Brest, P. Barbry, P.H., and J.R.; Methodology, R.W. and J.R.; Conceptualization, A.P. and J.R.; Writing – Original Draft, A.P. and J.R.; Writing – Review & Editing, A.P., M.-J.A., P. Brest, P. Barbry, K.L., R.W., and J.R.; Visualization, A.P. and J.R.; Funding Acquisition, J.R.; Supervision, J.R.

## DECLARATION OF INTERESTS

Methods and results presented here are part of a patent application (J.R., A.P., L.C.G.-P., and M.M.). Other authors declare no competing interests.

Received: March 2, 2020
Revised: June 12, 2020
Accepted: August 28, 2020
Published: September 23, 2020

## REFERENCES

Acar, M., Mettetal, J.T., and van Oudenaarden, A. (2008). Stochastic switching as a survival strategy in fluctuating environments. Nat. Genet. *40*, 471–475.

Adamson, B., Norman, T.M., Jost, M., Cho, M.Y., Nuñez, J.K., Chen, Y., Villalta, J.E., Gilbert, L.A., Horlbeck, M.A., Hein, M.Y., et al. (2016). A multiplexed single-cell CRISPR screening platform enables systematic dissection of the unfolded protein response. Cell *167*, 1867–1882.e21.

Albeck, J.G., Burke, J.M., Aldridge, B.B., Zhang, M., Lauffenburger, D.A., and Sorger, P.K. (2008). Quantitative analysis of pathways controlling extrinsic apoptosis in single cells. Mol. Cell *30*, 11–25.

Albeck, J.G., Mills, G.B., and Brugge, J.S. (2013). Frequency-modulated pulses of ERK activity transmit quantitative proliferation signals. Mol. Cell *49*, 249–261.

Angelidis, I., Simon, L.M., Fernandez, I.E., Strunz, M., Mayr, C.H., Greiffo, F.R., Tsitsiridis, G., Ansari, M., Graf, E., Strom, T.-M., et al. (2019). An atlas of the aging lung mapped by single cell transcriptomics and deep tissue proteomics. Nat. Commun. *10*, 963.

Arguel, M.J., Lebrigand, K., Paquet, A., Ruiz García, S., Zaragosi, L.E., Barbry, P., and Waldmann, R. (2017). A cost effective 5′ selective single cell transcriptome profiling approach with improved UMI design. Nucleic Acids Res. *45*, e48.

Balázsi, G., van Oudenaarden, A., and Collins, J.J. (2011). Cellular decision making and biological noise: from microbes to mammals. Cell *144*, 910–925.

Bell, C.C., Fennell, K.A., Chan, Y.C., Rambow, F., Yeung, M.M., Vassiliadis, D., Lara, L., Yeh, P., Martelotto, L.G., Rogiers, A., et al. (2019). Targeting enhancer switching overcomes non-genetic drug resistance in acute myeloid leukaemia. Nat. Commun. *10*, 2723.

Datlinger, P., Rendeiro, A.F., Schmidl, C., Krausgruber, T., Traxler, P., Klughammer, J., Schuster, L.C., Kuchler, A., Alpar, D., and Bock, C. (2017). Pooled CRISPR screening with single-cell transcriptome readout. Nat. Methods *14*, 297–301.

Dawson, M.A. (2017). The cancer epigenome: concepts, challenges, and therapeutic opportunities. Science *355*, 1147–1152.

Dixit, A., Parnas, O., Li, B., Chen, J., Fulco, C.P., Jerby-Arnon, L., Marjanovic, N.D., Dionne, D., Burks, T., Raychowdhury, R., et al. (2016). Perturb-seq: dissecting molecular circuits with scalable single-cell RNA profiling of pooled genetic screens. Cell *167*, 1853–1866.e17.

Dobin, A., Davis, C.A., Schlesinger, F., Drenkow, J., Zaleski, C., Jha, S., Batut, P., Chaisson, M., and Gingeras, T.R. (2013). STAR: ultrafast universal RNA-seq aligner. Bioinformatics *29*, 15–21.

Eling, N., Morgan, M.D., and Marioni, J.C. (2019). Challenges in measuring and understanding biological noise. Nat. Rev. Genet. *20*, 536–548.

Elowitz, M.B., Levine, A.J., Siggia, E.D., and Swain, P.S. (2002). Stochastic gene expression in a single cell. Science *297*, 1183–1186.

Fallahi-Sichani, M., Honarnejad, S., Heiser, L.M., Gray, J.W., and Sorger, P.K. (2013). Metrics other than potency reveal systematic variation in responses to cancer drugs. Nat. Chem. Biol. *9*, 708–714.

Flusberg, D.A., Roux, J., Spencer, S.L., and Sorger, P.K. (2013). Cells surviving fractional killing by TRAIL exhibit transient but sustainable resistance and inflammatory phenotypes. Mol. Biol. Cell *24*, 2186–2200.

Forcina, G.C., Conlon, M., Wells, A., Cao, J.Y., and Dixon, S.J. (2017). Systematic quantification of population cell death kinetics in mammalian cells. Cell Syst. *4*, 600–610.e6.

Friedman, J.R., Lackner, L.L., West, M., DiBenedetto, J.R., Nunnari, J., and Voeltz, G.K. (2011). ER tubules mark sites of mitochondrial division. Science *334*, 358–362.

Gonzalvez, F., and Ashkenazi, A. (2010). New insights into apoptosis signaling by Apo2L/TRAIL. Oncogene *29*, 4752–4765.

Holland, P.M. (2014). Death receptor agonist therapies for cancer, which is the right TRAIL? Cytokine Growth Factor Rev. *25*, 185–193.

Jaitin, D.A., Kenigsberg, E., Keren-Shaul, H., Elefant, N., Paul, F., Zaretsky, I., Mildner, A., Cohen, N., Jung, S., Tanay, A., and Amit, I. (2014). Massively parallel single-cell RNA-seq for marker-free decomposition of tissues into cell types. Science *343*, 776–779.

Karaayvaz, M., Cristea, S., Gillespie, S.M., Patel, A.P., Mylvaganam, R., Luo, C.C., Specht, M.C., Bernstein, B.E., Michor, F., and Ellisen, L.W. (2018). Unravelling subclonal heterogeneity and aggressive disease states in TNBC through single-cell RNA-seq. Nat. Commun. *9*, 3588.

Kim, C., Gao, R., Sei, E., Brandt, R., Hartman, J., Hatschek, T., Crosetto, N., Foukakis, T., and Navin, N.E. (2018). Chemoresistance evolution in triple-negative breast cancer delineated by single-cell sequencing. Cell *173*, 879–893.e13.

Lane, K., Van Valen, D., DeFelice, M.M., Macklin, D.N., Kudo, T., Jaimovich, A., Carr, A., Meyer, T., Pe'er, D., Boutet, S.C., and Covert, M.W. (2017). Measuring signaling and RNA-seq in the same cell links gene expression to dynamic patterns of NF-κB activation. Cell Syst. *4*, 458–469.e5.

Liu, C., He, H., Li, X., Su, M.A., and Cao, Y. (2019). Dynamic metrics-based biomarkers to predict responders to anti-PD-1 immunotherapy. Br. J. Cancer *120*, 346–355.

Loewer, A., Karanam, K., Mock, C., and Lahav, G. (2013). The p53 response in single cells is linearly correlated to the number of DNA breaks without a distinct threshold. BMC Biol. *11*, 114.

Lun, A.T.L., McCarthy, D.J., and Marioni, J.C. (2016). A step-by-step workflow for low-level analysis of single-cell RNA-seq data with Bioconductor. F1000Res. *5*, 2122.

Macosko, E.Z., Basu, A., Satija, R., Nemesh, J., Shekhar, K., Goldman, M., Tirosh, I., Bialas, A.R., Kamitaki, N., Martersteck, E.M., et al. (2015). Highly parallel genome-wide expression profiling of individual cells using nanoliter droplets. Cell *161*, 1202–1214.

Marusyk, A., Almendro, V., and Polyak, K. (2012). Intra-tumour heterogeneity: a looking glass for cancer? Nat. Rev. Cancer *12*, 323–334.

McCarthy, D.J., Chen, Y., and Smyth, G.K. (2012). Differential expression analysis of multifactor RNA-seq experiments with respect to biological variation. Nucleic Acids Res. *40*, 4288–4297.

Mitchell, S., Roy, K., Zangle, T.A., and Hoffmann, A. (2018). Nongenetic origins of cell-to-cell variability in B lymphocyte proliferation. Proc. Natl. Acad. Sci. USA *115*, E2888–E2897.

Paek, A.L., Liu, J.C., Loewer, A., Forrester, W.C., and Lahav, G. (2016). Cell-to-cell variation in p53 dynamics leads to fractional killing. Cell *165*, 631–642.

Purvis, J.E., Karhohs, K.W., Mock, C., Batchelor, E., Loewer, A., and Lahav, G. (2012). p53 dynamics control cell fate. Science *336*, 1440–1444.

Raj, A., and van Oudenaarden, A. (2008). Nature, nurture, or chance: stochastic gene expression and its consequences. Cell *135*, 216–226.

Ramirez, M., Rajaram, S., Steininger, R.J., Osipchuk, D., Roth, M.A., Morinishi, L.S., Evans, L., Ji, W., Hsu, C.H., Thurley, K., et al. (2016). Diverse drug-resistance mechanisms can emerge from drug-tolerant cancer persister cells. Nat. Commun. *7*, 10690.

Revinski, D.R., Zaragosi, L.E., Boutin, C., Ruiz-Garcia, S., Deprez, M., Thomé, V., Rosnet, O., Gay, A.S., Mercey, O., Paquet, A., et al. (2018). CDC20B is required for deuterosome-mediated centriole production in multiciliated cells. Nat. Commun. *9*, 4668.

Reyes, J., and Lahav, G. (2018). Leveraging and coping with uncertainty in the response of individual cells to therapy. Curr. Opin. Biotechnol. *51*, 109–115.

Roux, J., Hafner, M., Bandara, S., Sims, J.J., Hudson, H., Chai, D., and Sorger, P.K. (2015). Fractional killing arises from cell-to-cell variability in overcoming a caspase activity threshold. Mol. Syst. Biol. *11*, 803.

Rubin, A.J., Parker, K.R., Satpathy, A.T., Qi, Y., Wu, B., Ong, A.J., Mumbach, M.R., Ji, A.L., Kim, D.S., Cho, S.W., et al. (2019). Coupled single-cell CRISPR screening and epigenomic profiling reveals causal gene regulatory networks. Cell *176*, 361–376.e17.

Saint, M., Bertaux, F., Tang, W., Sun, X.M., Game, L., Köferle, A., Bähler, J., Shahrezaei, V., and Marguerat, S. (2019). Single-cell imaging and RNA sequencing reveal patterns of gene expression heterogeneity during fission yeast growth and adaptation. Nat. Microbiol. *4*, 480–491.

Salgia, R., and Kulkarni, P. (2018). The genetic/non-genetic duality of drug "resistance" in cancer. Trends Cancer *4*, 110–118.

Santos, S.D.M., Verveer, P.J., and Bastiaens, P.I.H. (2007). Growth factor-induced MAPK network topology shapes Erk response determining PC-12 cell fate. Nat. Cell Biol. *9*, 324–330.

Shaffer, S.M., Dunagin, M.C., Torborg, S.R., Torre, E.A., Emert, B., Krepler, C., Beqiri, M., Sproesser, K., Brafford, P.A., Xiao, M., et al. (2017). Rare cell variability and drug-induced reprogramming as a mode of cancer drug resistance. Nature *546*, 431–435.

Sharma, S.V., Lee, D.Y., Li, B., Quinlan, M.P., Takahashi, F., Maheswaran, S., McDermott, U., Azizian, N., Zou, L., Fischbach, M.A., et al. (2010). A chromatin-mediated reversible drug-tolerant state in cancer cell subpopulations. Cell *141*, 69–80.

Spencer, S.L., Gaudet, S., Albeck, J.G., Burke, J.M., and Sorger, P.K. (2009). Non-genetic origins of cell-to-cell variability in TRAIL-induced apoptosis. Nature *459*, 428–432.

Stoeckius, M., Hafemeister, C., Stephenson, W., Houck-Loomis, B., Chattopadhyay, P.K., Swerdlow, H., Satija, R., and Smibert, P. (2017). Simultaneous epitope and transcriptome measurement in single cells. Nat. Methods *14*, 865–868.

Stoeckius, M., Zheng, S., Houck-Loomis, B., Hao, S., Yeung, B.Z., Mauck, W.M., Smibert, P., and Satija, R. (2018). Cell Hashing with barcoded antibodies enables multiplexing and doublet detection for single cell genomics. Genome Biol. *19*, 224.

Stuart, T., Butler, A., Hoffman, P., Hafemeister, C., Papalexi, E., Mauck, W.M., Hao, Y., Stoeckius, M., Smibert, P., and Satija, R. (2019). Comprehensive integration of single-cell data. Cell *177*, 1888–1902.e21.

Stuart, T., and Satija, R. (2019). Integrative single-cell analysis. Nat. Rev. Genet. *20*, 257–272.

Su, Y., Wei, W., Robert, L., Xue, M., Tsoi, J., Garcia-Diaz, A., Homet Moreno, B., Kim, J., Ng, R.H., Lee, J.W., et al. (2017). Single-cell analysis resolves the cell state transition and signaling dynamics associated with melanoma drug-induced resistance. Proc. Natl. Acad. Sci. USA *114*, 13679–13684.

Suderman, R., Bachman, J.A., Smith, A., Sorger, P.K., and Deeds, E.J. (2017). Fundamental trade-offs between information flow in single cells and cellular populations. Proc. Natl. Acad. Sci. USA *114*, 5755–5760.

Süel, G.M., Garcia-Ojalvo, J., Liberman, L.M., and Elowitz, M.B. (2006). An excitable gene regulatory circuit induces transient cellular differentiation. Nature *440*, 545–550.

Please cite this article in press as: Meyer et al., Profiling the Non-genetic Origins of Cancer Drug Resistance with a Single-Cell Functional Genomics Approach Using Predictive Cell Dynamics, Cell Systems (2020), https://doi.org/10.1016/j.cels.2020.08.019



CellPress
OPEN ACCESS

## STAR★METHODS

### KEY RESOURCES TABLE

| REAGENT or RESOURCE | SOURCE | IDENTIFIER |
|---|---|---|
| Antibodies | | |
| A0251 anti-human Hashtag 1 Antibody | Biolegend | cat# 394601 |
| A0252 anti-human Hashtag 2 Antibody | Biolegend | cat# 394603 |
| A0253 anti-human Hashtag 3 Antibody | Biolegend | cat# 394605 |
| A0254 anti-human Hashtag 4 Antibody | Biolegend | cat# 394607 |
| A0255 anti-human Hashtag 5 Antibody | Biolegend | cat# 394609 |
| ANTI-DR5 (PRO95780 (DROZITUMAB)) HUMAN IGM | Interchim | cat# AB00740-15.0 |
| Mapatumumab | Creative biolabs | cat# TAB-H48 |
| AffiniPure F(ab')$_2$ Fragment Donkey Anti-Human IgG, Fc$\gamma$ fragment specific | Jackson ImmunoResearch Europe Ltd | RRID: AB_2340485, cat# 709-006-098 |
| Bacterial and Virus Strains | | |
| pQCXIX (retroviral vector) | Clontech Takara Bio | cat# 631515 |
| pQCXIX mCherry (retroviral vector) | this manuscript | N/A |
| pQCXIX mCherry-DNM1L (retroviral vector) | this manuscript | N/A |
| pMSCV-pBabeMCS-IRES-RFP (retroviral vector) | Addgene | RRID: Addgene_33337 |
| pMSCV-BLOC1S1-IRES-RFP (retroviral vector) | this manuscript | N/A |
| pMSCV-LLPH-IRES-RFP (retroviral vector) | this manuscript | N/A |
| pMSCV-PRSS56-IRES-RFP (retroviral vector) | this manuscript | N/A |
| pMSCV-SIVA1-IRES-RFP (retroviral vector) | this manuscript | N/A |
| pMSCV-SLC25A1-IRES-RFP (retroviral vector) | this manuscript | N/A |
| pMSCV-UBE2D4-IRES-RFP (retroviral vector) | this manuscript | N/A |
| pMSCV-UQCC3-IRES-RFP (retroviral vector) | this manuscript | N/A |
| Chemicals, Peptides, and Recombinant Proteins | | |
| Cycloheximide | R&D Systems Europe | cat# 0970 |
| Dynasore | ENZO Life Science | cat# ALX-270-502 |
| Mdivi-1 | ENZO Life Science | cat# BML-CM127 |
| Hoechst 33342 dye | Thermo Fisher Scientific | cat# H3570 |
| Recombinant human (rh) TRAIL | R&D Systems Europe | cat# 375-TEC/CF |
| Tin protoporphyrin IX dichloride | R&D Systems Europe | cat# 0747 |
| Critical Commercial Assays | | |
| Master Mix Fast SYBR green | Thermo Fisher Scientific | cat# 4385618 |
| CellTiter-Glo Luminescent Assay | Promega | cat# G7570 |
| Chromium Single Cell 3' Reagent Kit, V2 Chemistry | 10X Genomics | cat# 120237 |
| RNeasy kit | Qiagen | cat# 74106 |
| High-Capacity cDNA Reverse Transcription Kit | Thermo Fisher Scientific | cat# 4368813 |
| Deposited Data | | |
| 10X Genomics, RNA sequencing processed data files | this manuscript | Mendeley data Dataset: https://doi.org/10.17632/m289yp5skd.1 |
| Fate-seq differential analysis results (edgeR) | this manuscript | Table S2 |
| 10X Genomics differential analysis results from the pseudo-bulk analyses (TRAIL time, dose) | this manuscript | Table S3 |
| fate-seq RNA sequencing raw data GEO, GSE138832 | this manuscript | https://www.ncbi.nlm.nih.gov/geo/query/acc.cgi?acc=GSE138832 |
| 10X Genomics, RNA sequencing raw data GEO, GSE138833 | this manuscript | https://www.ncbi.nlm.nih.gov/geo/query/acc.cgi?acc=GSE138833 |

(*Continued on next page*)

Please cite this article in press as: Meyer et al., Profiling the Non-genetic Origins of Cancer Drug Resistance with a Single-Cell Functional Genomics Approach Using Predictive Cell Dynamics, Cell Systems (2020), https://doi.org/10.1016/j.cels.2020.08.019



*Continued*

| REAGENT or RESOURCE | SOURCE | IDENTIFIER |
|---|---|---|
| Experimental Models: Cell Lines | | |
| HeLa IC-RP, mCherry (human) | this manuscript | N/A |
| HeLa IC-RP, mCherry-DNM1L (human) | this manuscript | N/A |
| HeLa IC-RP, RFP (human) | this manuscript | N/A |
| HeLa IC-RP, BLOC1S1, RFP (human) | this manuscript | N/A |
| HeLa IC-RP, LLPH, RFP (human) | this manuscript | N/A |
| HeLa IC-RP, PRSS56, RFP (human) | this manuscript | N/A |
| HeLa IC-RP, SIVA1, RFP (human) | this manuscript | N/A |
| HeLa IC-RP, SLC25A1, RFP (human) | this manuscript | N/A |
| HeLa IC-RP, UBE2D4, RFP (human) | this manuscript | N/A |
| HeLa IC-RP, UQCC3, RFP (human) | this manuscript | N/A |
| HeLa IC-RP (human) | (Roux et al., 2015) | N/A |
| Oligonucleotides | | |
| Target gene primers for qPCR | this manuscript | Table S7 |
| Cell ID barcodes | this manuscript | Table S4 |
| Isolated single cell library primers | this manuscript | Table S5 |
| Target gene primers for cloning | this manuscript | Table S6 |
| Software and Algorithms | | |
| Ingenuity Pathway Analysis (IPA, QIAGEN Inc). | QIAGEN Inc | https://digitalinsights.qiagen.com/ |
| R code for RNA sequencing data analyses | this manuscript | Github repository: https://github.com/jrxlab/fate-seq_proc |
| STAR | (Dobin et al., 2013) | v2.4.0a |
| Drop-seq tools | (Macosko et al., 2015) | v1.0 |
| ImageJ | https://imagej.nih.gov/ij/ | v1.5.2 |
| Fiji | https://fiji.sc/ | v2 |
| Cell Ranger Single-Cell Software Suite | 10X Genomics | v3.0.2 |
| R | https://www.r-project.org/ | v3.6.1 |

## RESOURCE AVAILABILITY

### Lead Contact

Further information and requests for resources and reagents should be directed to and will be fulfilled by the Lead Contact, Jeremie Roux (jeremie.roux@univ-cotedazur.fr).

### Materials Availability

Plasmids and cell lines generated in this study are available from the Lead Contact upon request, with an MTA when required.

### Data and Code Availability

10X Genomics RNA sequencing processed data files have been deposited to Mendeley Data (https://doi.org/10.17632/m289yp5skd.1). Fate-seq RNA sequencing and 10X Genomics raw data can be accessed on GEO (accession # GSE138832 and GSE138833 respectively): https://www.ncbi.nlm.nih.gov/geo/query/acc.cgi?acc=GSE138832, https://www.ncbi.nlm.nih.gov/geo/query/acc.cgi?acc=GSE138833.

R code for RNA sequencing data analyses is available at: https://github.com/jrxlab/fate-seq_proc.

## EXPERIMENTAL MODEL

HeLa cells (derived from human, female cervix adenocarcinoma) were obtained from the ATCC and cultured in DMEM Glutamax supplemented with 10% fetal bovine serum and penicillin/streptomycin (Thermo Fisher Scientific, France) or in phenol red-free DMEM Glutamax supplemented with 10% fetal bovine serum and penicillin / streptomycin (Thermo Fisher Scientific, France) during live-cell imaging. The parental cells and its derived subclones and engineered cell lines tested negatively for mycoplasma contamination.

Please cite this article in press as: Meyer et al., Profiling the Non-genetic Origins of Cancer Drug Resistance with a Single-Cell Functional Genomics Approach Using Predictive Cell Dynamics, Cell Systems (2020), https://doi.org/10.1016/j.cels.2020.08.019



## METHOD DETAILS

### Plasmids and Cloning

mRFP1 versions of *BLOC1S1*, *DNM1L*, *LLPH*, *PRSS56*, *SIVA1*, *SLC25A1*, *UBE2D4*, *UQCC3* (*C11orf83*) were constructed by PCR from ORF Clones in pcDNA3.1+/C-(K)-DYK vectors (GenScript Biotech B.V., Netherlands) or from mCh-Drp1 (a gift from Gia Voeltz (Friedman et al., 2011), Addgene plasmid # 49152), all with mRFP1 in position 2 after the IRES (transcriptional fusion) in pMSCV-pBabeMCS-IRES-RFP (a gift from Martine Roussel & Charles Sherr , Addgene plasmid # 33337) and in pQCXIX (Clontech Takara Bio, France). Primers for subcloning can be found in Table S6.

### Cell Line Constructions

HeLa cells stably expressing IC-RP (Roux et al., 2015) were used for all cell lines constructions, freshly cloned cells were used in all experiments (below passage 10). *BLOC1S1*, *DNM1L*, *LLPH*, *PRSS56*, *SIVA1*, *SLC25A1*, *UBE2D4*, *UQCC3* (*C11orf83*) with mRFP1 cells (transcriptional fusion) were obtained by infection with retrovirus (Retro-X system, Clontech Takara Bio, France) of the respective mRFP1 fusion gene into the parental clone of HeLa IC-RP cells. After infection, positive cells were enriched by FACS sorting but not sub-cloned to avoid the selection of a particular clone and to allow the emergence of a population of cells expressing various amount of each mRFP1 tagged protein.

### Quantitative PCR

Cells were washed twice with cold PBS, lysed and frozen in Trizol (TR-118; Euromedex, Souffelweyersheim, France). RNA was extracted using a RNeasy kit (74106, QIAGEN Inc). RNA concentration was determined by measuring absorbance at 260/280 nm. RNA was reverse transcribed to cDNA using High-Capacity cDNA Reverse Transcription Kit (4368813; Thermo Fisher Scientific, France). Quantitative PCR was performed with 50 ng cDNA, 500 nM primer, and Master Mix Fast SYBR green (4385618; Thermo Fisher Scientific, France). Primers are listed in the Table S7.

### Cell Viability

Viable cells were determined using CellTiter-Glo® Luminescent Assay (Promega, Madison, USA) or directly counted using Hoechst stain. Briefly, $2\times10^3$ cells/well were added to the 96-well plate before being treated 24 hr later with TRAIL in a DMEM medium supplemented with 10% of FBS. After 15 hours of TRAIL treatment, the CellTiter-Glo® buffer and substrate, but also the 96-well plate were all equilibrated to room temperature prior to use. Buffer and substrate were mixed and a volume equal to the volume of cell culture medium present in each well, was directly added to the plate. The plate was then mixed on an orbital shaker to induce cell lysis and finally read with a luminometer (2104 EnVision® Multilabel Plate Reader, PerkinElmer). For Hoechst staining, a final concentration of 2.5 μg/ml Hoechst 33342 dye (Thermo Fisher Scientific, France) was added after the TRAIL treatment, to each well and incubated for 15 min in the dark at 37°C. Finally, the viability was quantified on images acquired with a fluorescence microscope (EVOS FL, AMG with 10x magnification), using Fiji software.

### Clonogenic Assays

Cells were plated on a 96-well plate. After 24h, there were treated with a saturating dose of TRAIL (250ng/mL) and let grown for colony formation. After one week medium was removed and wells were washed with PBS. Colonies were both fixed and stained with a solution of 3.7% paraformaldehyde and 0.5% crystal violet in phosphate-buffered saline (PBS, pH 7.2) for 30 minutes, then washed three times with PBS. The 96-well plate was kept at room temperature and quantified using Fiji software.

### Live-Cell Microscopy

Clonal HeLa cells stably expressing the FRET-based initiator caspase reporter (IC-RP) were seeded into FrameSlides PET (Carl Zeiss, France) or 96-well plates, coated with rat-tail collagen I (Thermo Fisher Scientific, France). Cells in phenol red-free DMEM Glutamax supplemented with 10% fetal bovine serum and penicillin / streptomycin (Thermo Fisher Scientific, France), were imaged every 3 min for up to 24 hours in the temperature/CO2-controlled environmental chamber of a DeltaVision Elite microscope (GE Healthcare Life Sciences, Velizy-Villacoublay, France), with a 20x objective (NA = 0.75) in transmitted light and using the following solid-state illumination excitation wavelengths and single bandpass emission filters : for CFP (Ex. 438/24 nm / Em. 475-24 nm), YFP (Ex. 513/17 nm / Em. 548/22 nm). In addition to the time-lapse runs, cells stably expressing our target proteins tagged with mRFP1 or mCherry, were imaged at the beginning of the experiment for mCherry (Ex. 575/25 nm / Em. 625-45 nm).

### Laser-Capture Microdissection

Right after a 50-minute live-cell microscopy, the reaction was stopped by replacing the FrameSlide cell media with PBS Ca2+/Mg2+ at 4dC, and non-contact laser capture microdissection was performed with a Zeiss PALM MicroBeam (Carl Zeiss, France). Cells were ranked based on their caspase-8 activation rates at 50 minutes, determined by live-cell microscopy image and signal analyses, to select high and low responding cells, and their xy coordinates were converted to position the Zeiss RoboStage accordingly (using scripts developed in house). Chosen single-cells were then catapulted into 0.2 ml domed caps tube (strips) containing 4.3 μl of lysis buffer (0,2% w/v Tween 20, 1.5U/μl Promega RNAseIN Plus). Tubes were kept on ice and frozen in dry ice directly after collection to minimize RNA degradation during sample collection and transport.

Please cite this article in press as: Meyer et al., Profiling the Non-genetic Origins of Cancer Drug Resistance with a Single-Cell Functional Genomics Approach Using Predictive Cell Dynamics, Cell Systems (2020), https://doi.org/10.1016/j.cels.2020.08.019



### Laser-Captured Single-Cell Sequencing

#### *cDNA Preparation*

Samples were thawed on ice and 2.43 μl of a mix containing 10,000 molecules Life Technologies ERCC spike-In Mix 1, 2.5 mM dNTPs, and 3.7 μM single barcoded reverse transcription primer (Table S4) was added to each tube, incubated for 10 min at room temperature, 3 min at 70°C and cooled to 10°C. Immediately after lysis, 8.27 μl 1.8X reverse transcription buffer (Invitrogen), 4.53 mM DTT, 1.8M Betaïne, 10.8 mM MgCl2, 3.62 μM template switching oligonucleotide, 0.6 U/μl Promega RNAse IN Plus, 7.5 U/μl Invitrogen SuperScript II reverse transcriptase were added and samples were reverse transcribed 10 min at 25°C, 90 min at 42°C, 15 min at 70°C and kept at 10°C until PCR amplification. Samples were PCR amplified (KAPA HiFi Hotstart) in 31 μl for 20 cycles with 0.8 μM forward PCR primer, 0.8 μM biotinylated reverse PCR primer (primer sequences in Table S5). Samples were incubated 3 min at 98°C followed by 20 cycles at 98°C for 20 sec, 64°C for 15 sec, 72°C for 6 min followed by a final extension for 5 min at 72°C. After PCR amplification, samples were pooled and purified with 0.8X Beckman Coulter SPRIselect beads, washed once with 85% EtOH and eluted in 30 μl.

#### *Library Preparation*

Batches of barcoded cDNAs were pooled, purified with SPRIselect beads (0.8x) and eluted in 12 μl. Nine μl (typically 10 – 20 ng of cDNA) were used for tagmentation and Illumina library preparation as previously described (Arguel et al., 2017).

#### *Sequencing*

Libraries were sequenced with a NextSeq 500/550 High Output v2 kit (75 cycles) that allows up to 91 cycles with an index1 read of 20 nt. (8-bp cell barcode and 12 bp UMI) and a read1 of 71 nt. for cDNA sequencing, with custom sequencing primers as described in (Arguel et al., 2017).

### Droplet-based Single-Cell Sequencing

#### *Single-Cell Preparation*

Clonal HeLa cells stably expressing the FRET-based initiator caspase reporter (IC-RP) were cultured in 6-well plates for 24 hours and then treated with TRAIL. Right after treatments, cells from each treatment conditions, were detached with trypsin (filtered, counted) and incubated with Hashtag antibodies (Biolegend TotalSeq™, San Diego, CA) for 20 min at 4 dC. Live cells from each treatment conditions were then counted and merged into one sample according to the manufacturer's recommendations (10x Genomics, Netherlands). Cell Hashing protocol with Hashtag oligonucleotide (HTO) was then conducted with 10x Genomics single-cell 3' V2 chemistry to generate single-cell emulsion.

#### *Single-Cell and Hashtag Oligo Sequencing*

Single-cell RNA-seq was performed following manufacturer's protocol (Chromium™ Single Cell 3' Reagent Kit, V2 Chemistry) to obtain single cell 3' libraries for Illumina sequencing. PCR of 12 cycles was performed for cDNA amplification with HTO primer (Stoeckius et al., 2018). Final cDNA library was then pooled with 10% of HTO library in final pool for sequencing.

Libraries were sequenced with a NextSeq 500/550 High Output v2 kit (75 cycles) that allows up to 91 cycles of paired-end sequencing: Read 1 had a length of 26 bases that included the cell barcode and the UMI; Read 2 had a length of 57 bases that contained the cDNA insert; Index reads for sample index of 8 bases. Cell Ranger Single-Cell Software Suite v3.0.2 was used to perform demultiplexing of individual cells, barcode processing and single-cell 3′ gene counting using standards default parameters and human build GRCh38.

#### *Hashtag Library Preparation and Analysis*

For HTO library preparation, 10 cycles of PCR amplification (Stoeckius et al., 2018) followed by a size selection with Blue Pippin 3% agarose gel cassette (BDQ3010) Marker Q3 were necessary to select 180bp specific amplicon. We used the following sample barcodes from BioLegend: A0251: GTCAACTCTTTAGCG, A0252: TGATGGCCTATTGGG, A0253: TTCCGCCTCTCTTTG, A0254: AGTAAGTTCAGCGTA, A0255: AAGTATCGTTTCGCA. Antibody hashtags counting was done using CITE-seq-Count (Stoeckius et al., 2017) using standard 10X Genomics parameters "-cbf 1 -cbl 16 -umif 17 -umil 26 -hd 2" and barcode "–whitelist" from Cell Ranger analysis.

## QUANTIFICATION AND STATISTICAL ANALYSIS

### Live-Cell Imaging Analyses

For the analysis of the FRET signal, the background-subtracted CFP and YFP images were divided to get a ratiometric image (CFP/YFP) using ImageJ and custom plug-ins to track cells (Albeck et al., 2008). Signals were normalized by subtracting the minimum value across all time points from each single-cell time course and the average trajectory of the corresponding drug vehicle-treated cells. Cell death times were determined by visual inspection, for each corresponding cell trajectory with the transmitted light image stacks and used to determine population cell viability. Cell death assessment was performed by visual inspection in transmitted light of the cell morphology change, cell death time was marked and used for cell death counts. Caspase-8 activation rates were determined from CFP/YFP ratio trajectories, as described before (Roux et al., 2015).

#### *Statistical Analyses on Live-Cell Experiments*

Independent replicate numbers (n) are reported in the corresponding figure panels. Statistical significance of the difference in maximal activation rates was assessed using Wilcoxon rank sum test, statistical significance of the surviving fractions in experiments repeats was assessed using two-sample t-test, and Cell Survival probabilities (Empirical Survivor Function, ecdf) were compared with a two-sample Kolmogorov-Smirnov test.

Please cite this article in press as: Meyer et al., Profiling the Non-genetic Origins of Cancer Drug Resistance with a Single-Cell Functional Genomics Approach Using Predictive Cell Dynamics, Cell Systems (2020), https://doi.org/10.1016/j.cels.2020.08.019



## Laser-Captured Single-Cell Analyses

### *Bioinformatics Analyses*

Mapping of cDNA reads was performed using STAR against human hg19 build following encode RNA-seq recommendations (Dobin et al., 2013). Drop-seq tools (Macosko et al., 2015) was then used to tag SAM records with cell barcode (XC) and molecule identifier (XM) extracted from index1 reads. Gene name tag (GE) were also added using Drop-seq (TagReadWithGeneExon pipeline) and Ensembl reference GRCh37.75 prior to digital expression count matrix production using an edit distance of 1 (DigitalExpression pipeline).

## Statistical Analyses

Exploratory analysis of single-cell RNA-seq data was performed for quality control. Poor quality cells, based on high dropout rate and outlier total UMI counts (number of UMI < 40,000 or > 220,000), were excluded from the final dataset to avoid including damaged cells and doublets that could not be detected during laser capture microdissection. Library size normalization and highly variable genes selection were performed using the R package scran (Lun et al., 2016). Cell-cycle assessment was performed using the algorithm described before (Macosko et al., 2015), based on our curated gene sets (Revinski et al., 2018). Hierarchical clustering and heatmaps were generated using the R package pheatmap, using Euclidean distance and Ward.D method unless otherwise specified. Differential analysis was performed using the edgeR likelihood ratio test framework (McCarthy et al., 2012). P-values were adjusted for multiple testing using the Benjamini-Hochberg method. Molecular function enrichment analyses were performed using Ingenuity Pathway Analysis (IPA, QIAGEN Inc).

## Droplet-based Single-Cell Analyses

### *Hashtag Demultiplexing and Preprocessing*

Single-cell RNA-seq and hashtag data were analyzed using the R toolkit Seurat V3 (Stuart et al., 2019) and custom R scripts. Hashtag counts were normalized using the CLR method, then cell barcodes were demultiplexed and doublet and negative cells were excluded using the HTODemux function with parameter positive.quantile = 0.95. Low quality cells were excluded from the dataset based on the following criteria: number of genes detected < 2,000, percentage of UMI mapping to mitochondrial genes > 5% or number of UMIs < 10,000. The final numbers of cells included were: 1,529 for control sample, 1,481 for TRAIL 50 min 25 ng/ml, 1,631 for TRAIL 120 min 10 ng/ml, 1,804 for TRAIL 120 min 25 ng/ml and 2,115 for TRAIL 120 min 40 ng/ml. Cell cycle scores were calculated using Seurat CellCycleScoring function, based on previously published gene sets (Revinski et al., 2018). Each sample was first normalized to 10,000 UMIs, and variable features were selected using the vst method.

### *Analysis of Control and TRAIL 50-min Samples*

Analysis of individual samples was performed using the standard Seurat workflow based on a number of PC = 10 and SNN/Louvain clustering with resolution parameter res=0.3.

### *Integration of Control and Treated Samples*

We used the Seurat V3 data integration pipeline to analyze all 5 samples together (Stuart et al., 2019). Integration was performed based on the first 20 CCA dimensions, and a regression of the G2M, S scores and total number of RNA molecules was included to remove the effects of cell cycle and sequencing depth. PCA was used as dimensionality reduction technique, and the number of PCs to include in downstream analyses was set based on inspection of the elbow plot. A resolution of 0.1 was used for the SNN/Louvain clustering. Significance of differential expression analysis between clusters or between experimental conditions was performed using Wilcoxon Rank Sum test using the FindMarker function. MA-plot between experimental conditions were generated using average gene expression values estimated using the AverageExpression function.

### *Pseudo-Bulk Analysis*

Two pseudo-bulk samples were constructed from each single cell sample by randomly selecting 700 cells (without replacement) among all cells passing quality filter, then, we calculated the UMI count value for each gene by adding the UMIs counts corresponding to this gene from these 700 cells. Statistical analysis of bulk samples was performed using the R package edgeR (McCarthy et al., 2012). Library size differences normalization factors were calculated using the TMM method. Differential analysis was performed using the likelihood ratio test. Pvalues were adjusted for multiple testing using the Benjamini-Hochberg method. Heatmaps were generated using the R package pheatmap. Gene set enrichment analysis was performed using the package fgsea.

### *Transcriptional Noise Analysis*

Raw single cell count data was used for this analysis. The following preprocessing was applied in order to account for differences in sequencing depth for each cell and for differences in the number of single-cell captured for each sample. First, we started by randomly selecting 1000 cells among all cells with at least 15,000 UMIs in each sample. Then, for each cell, the number of UMIs was downsampled to 15,000 using the SampleUMI function in Seurat. For each sample, the transcriptional noise was measured as 1- rho, where rho is the Spearman correlation coefficient between 2 cells, for all possible pairs of cells in this sample (Angelidis et al., 2019).

**Cell Systems, Volume *11***

## Supplemental Information

# Profiling the Non-genetic Origins of Cancer Drug Resistance with a Single-Cell Functional Genomics Approach Using Predictive Cell Dynamics

**Mickael Meyer, Agnès Paquet, Marie-Jeanne Arguel, Ludovic Peyre, Luis C. Gomes-Pereira, Kevin Lebrigand, Baharia Mograbi, Patrick Brest, Rainer Waldmann, Pascal Barbry, Paul Hofman, and Jérémie Roux**

**Cell Systems, Volume *11***

## Supplemental Information

# Profiling the Non-genetic Origins of Cancer Drug Resistance with a Single-Cell Functional Genomics Approach Using Predictive Cell Dynamics

**Mickael Meyer, Agnès Paquet, Marie-Jeanne Arguel, Ludovic Peyre, Luis C. Gomes-Pereira, Kevin Lebrigand, Baharia Mograbi, Patrick Brest, Rainer Waldmann, Pascal Barbry, Paul Hofman, and Jérémie Roux**

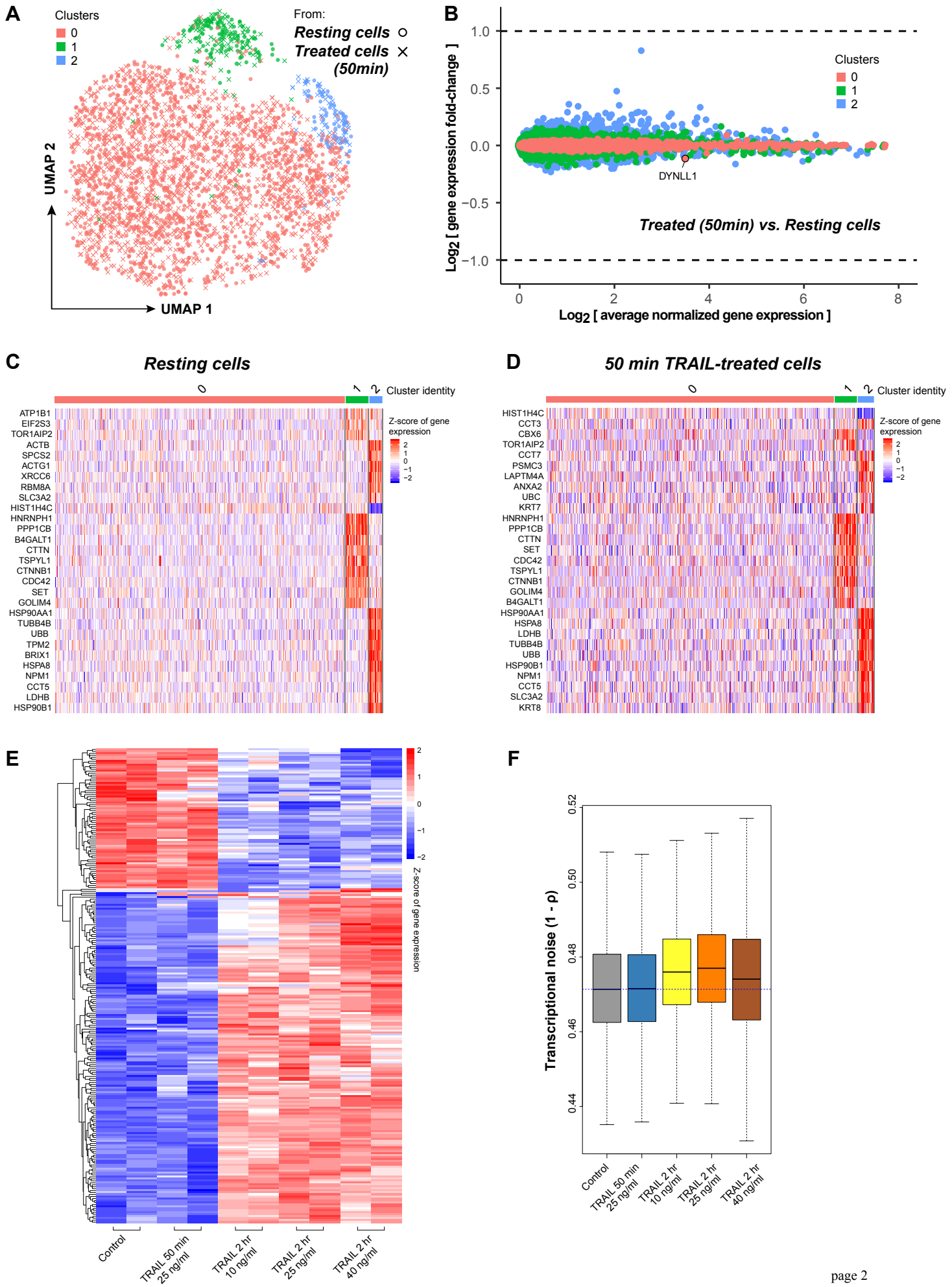




Supplementary Figure 1

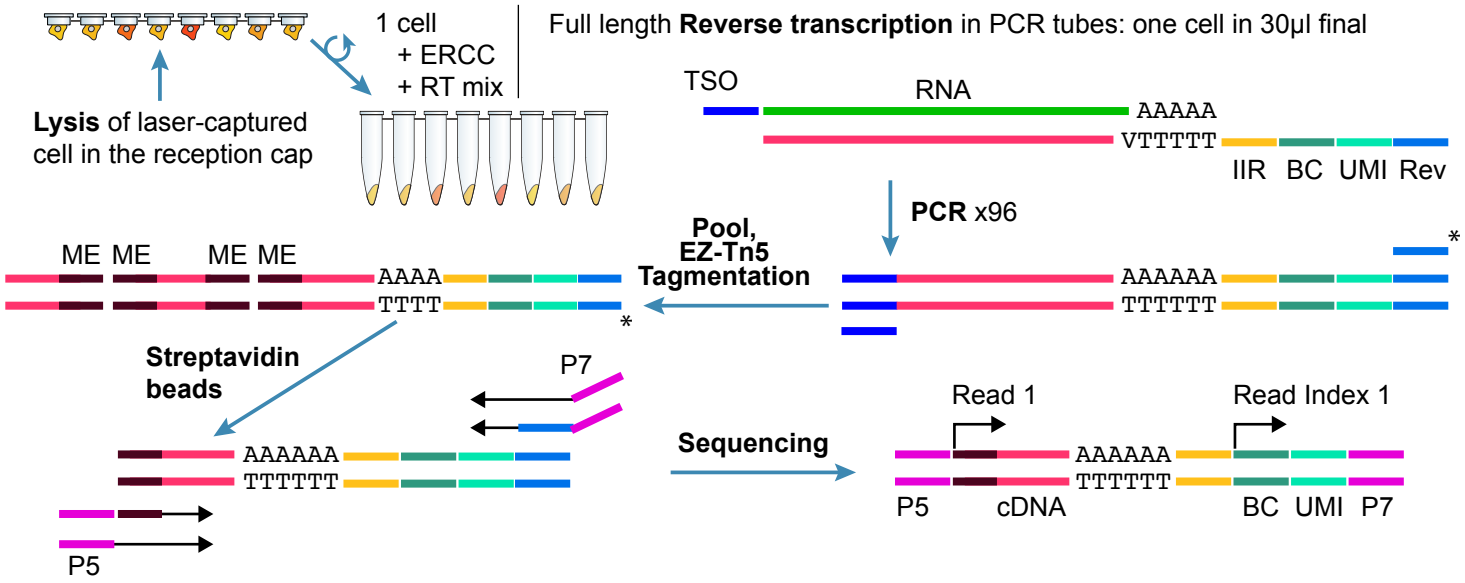




Supplementary Figure 2

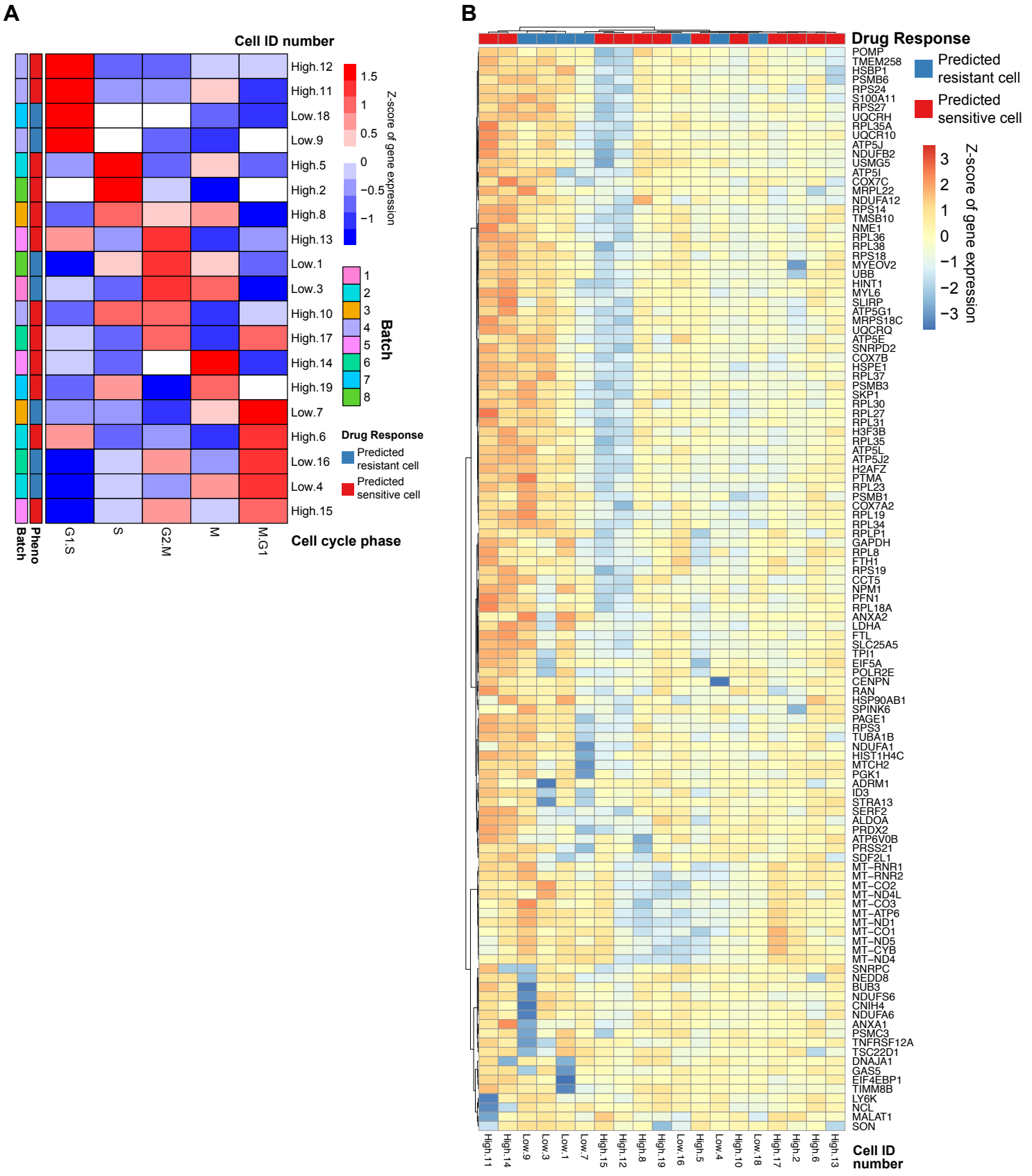




Supplementary Figure 3

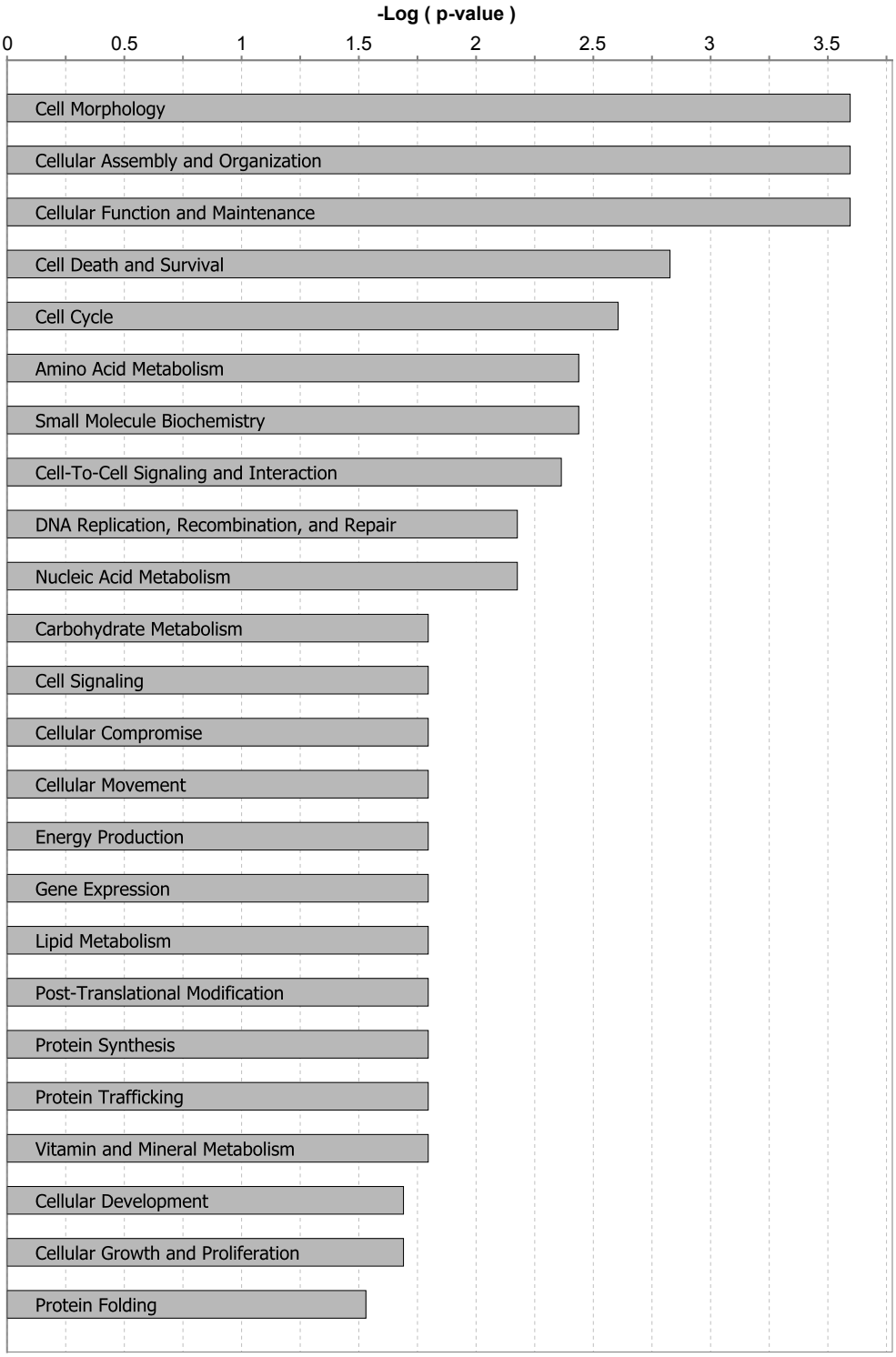




Supplementary Figure 4

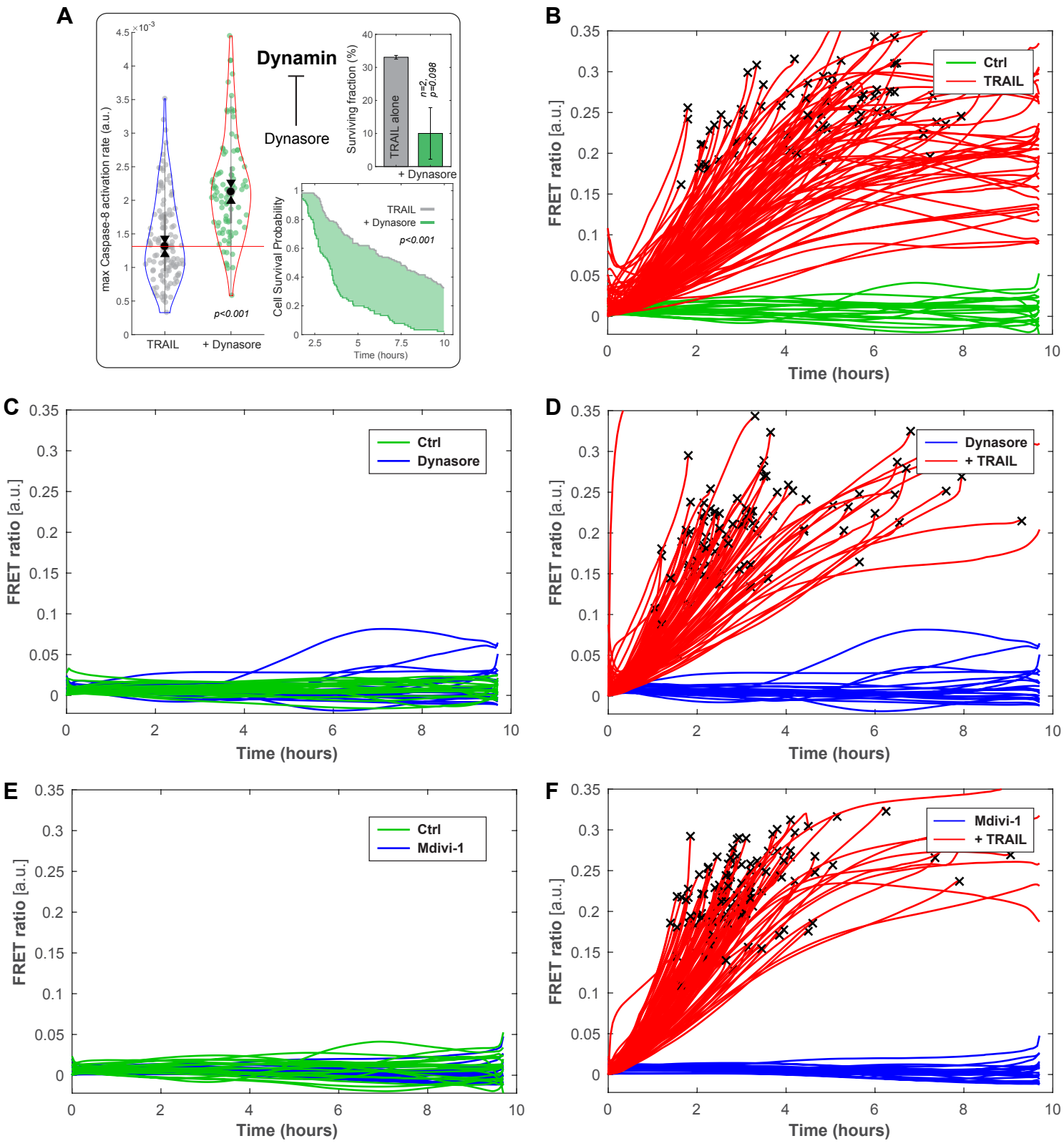


Supplemental Information

page 6

Supplementary Figure 5

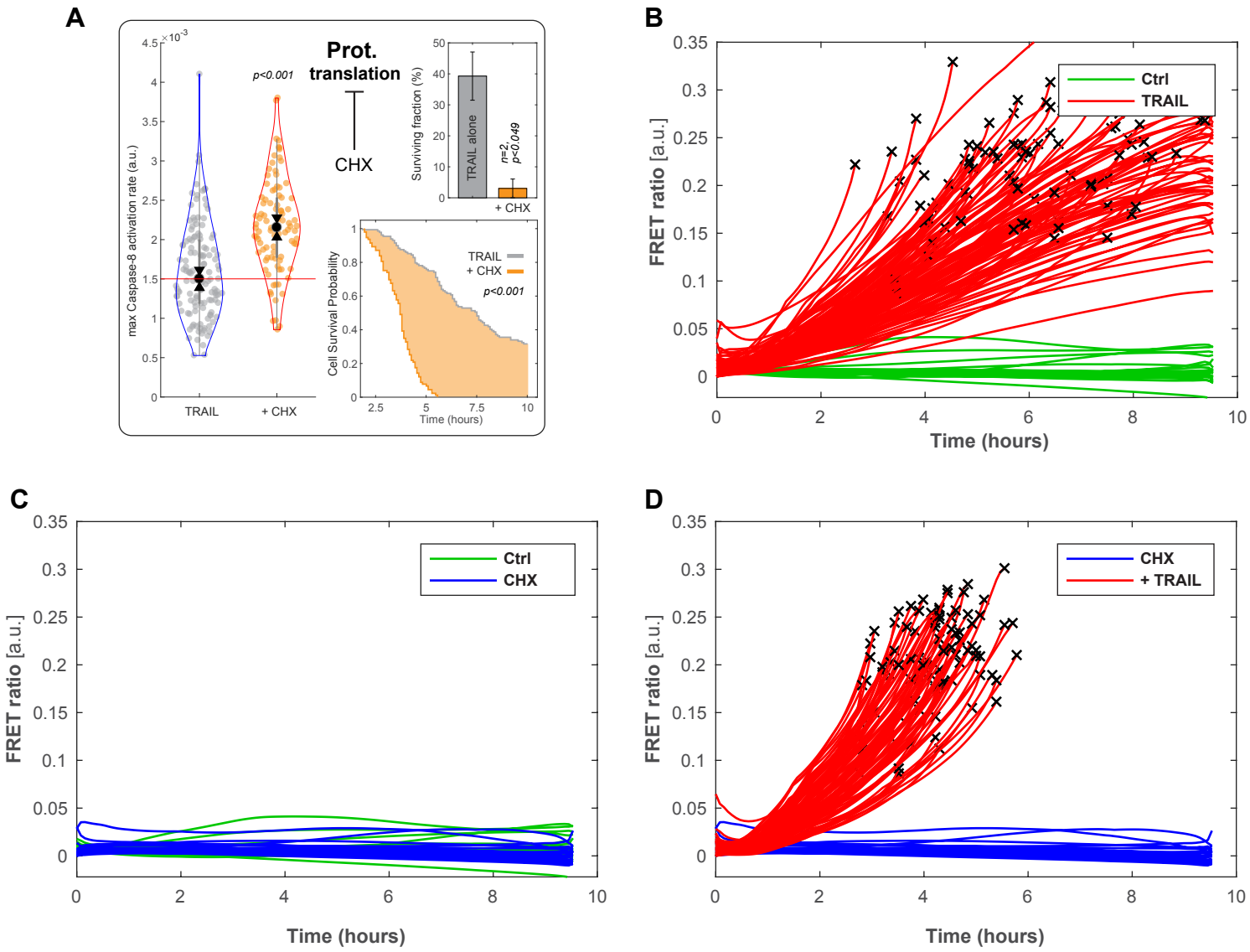




Supplementary Figure 6

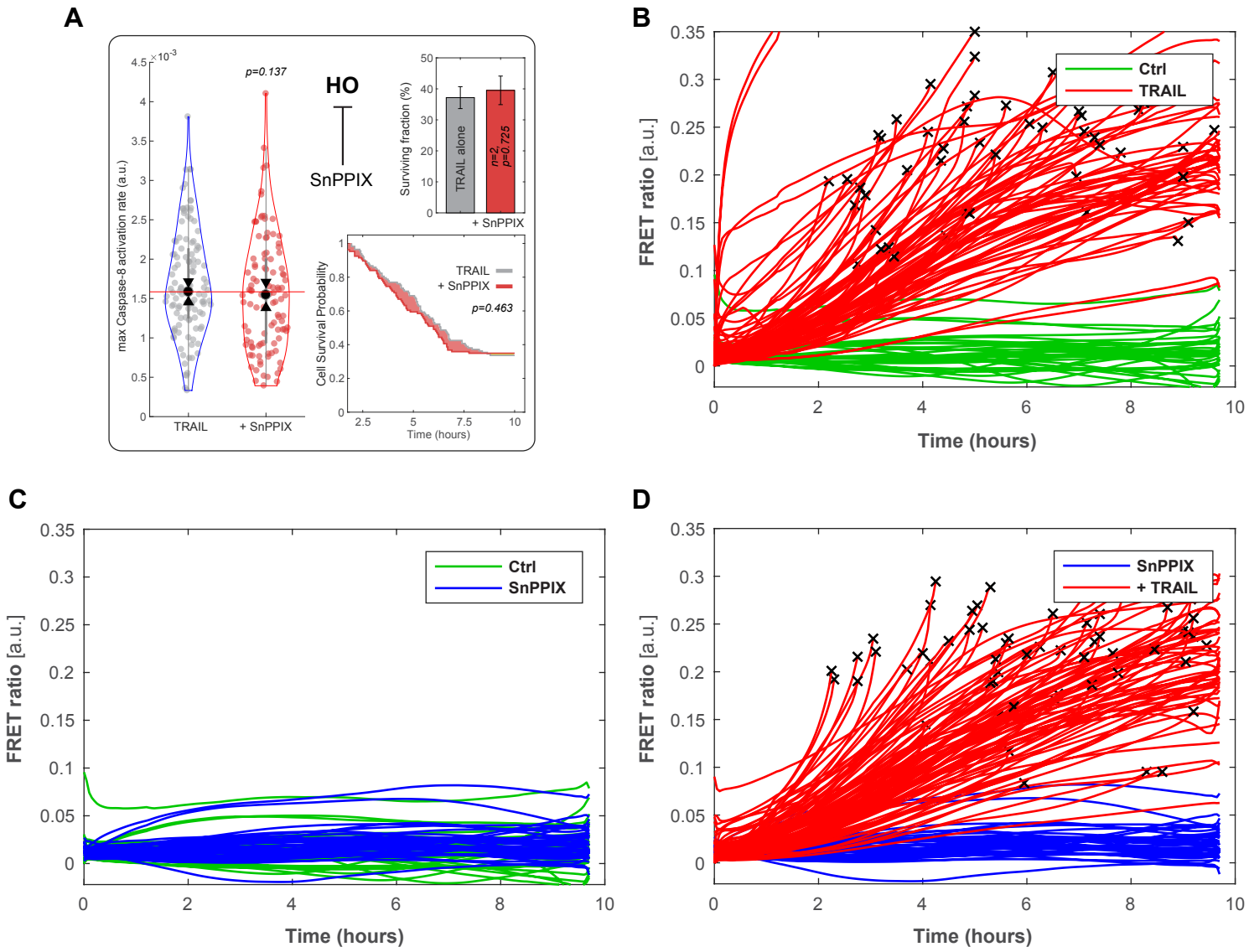




Supplementary Figure 7

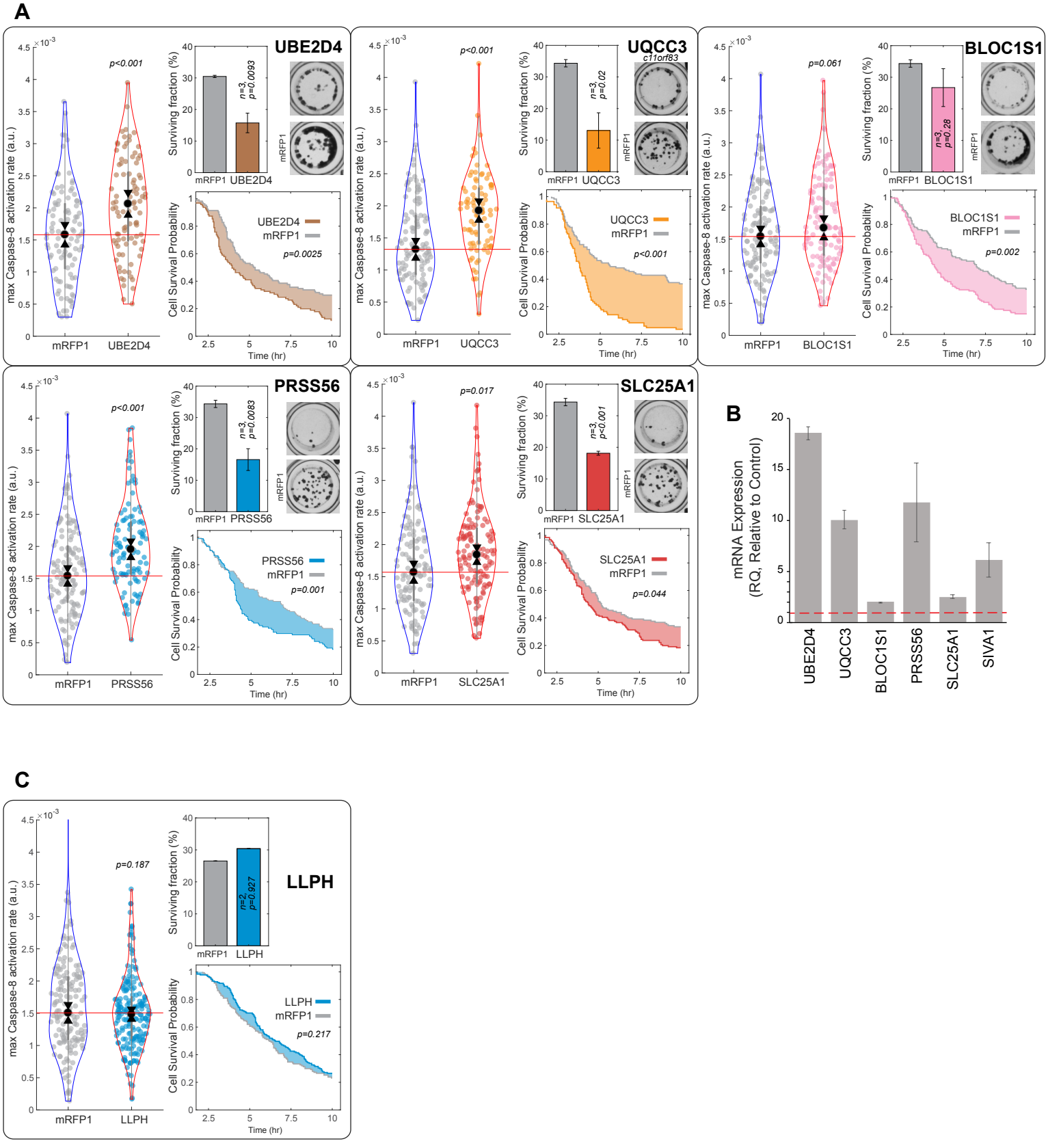




Supplementary Figure 8

**Figure S1: Single-cell RNAseq profiling of HeLa cells in resting conditions or after short treatment with TRAIL.** Related to Figure 1

(**A**) UMAP representation of the joint analysis of control resting cells and 50-min treated cells, profiled using the 10X Genomics platform (> 1,500 cells per condition). Three cell sub-populations were found by clustering analysis after regressing out the cell cycle component.

(**B**) Differential analysis of the 50-min treated cells vs. control resting cells, for each of the 3 cell sub-population clusters observed in panel A. The x-axis: average normalized gene expression in a given cluster (log2 scale). The y-axis: log2 fold-change of gene expression between 50-min treated cells and control. Only one gene, *DYNLL1*, reached statistical significance after adjustment for multiple testing.

(**C**) Heatmap of the most differentially expressed (DE) genes by clusters, for the resting cells.

**(D**) Heatmap of the most DE genes by clusters, after a 50-min treatment with TRAIL 25 ng/ml.

(**E**) Pseudo-bulk RNAseq analysis of response to increasing time and dose of TRAIL treatment. The heatmap is based on a subset of 241 genes found differentially expressed after 120 min treatment with TRAIL, at 10 ng/ml, 25 ng/ml and 40 ng/ml (Table S3). It required 2 hours to start detecting some DE genes in HeLa cells treated with TRAIL, with only the TNF signaling hallmark pathway showing significant enrichment (GSEA with FDR < 0.1, Table S3). No gene was found statistically significant when comparing TRAIL 50 min at 25ng/ml with control.

(**F**) Gene expression noise analysis. Each boxplot represents the distribution of the transcription noise measured in each condition. No difference was observed between control and TRAIL 25 ng/ml for 50 min, and only a slight increase is observed in the other conditions.

**Figure S2: Isolated single cell library preparation for RNA sequencing.** Related to Figure 1

Laser captured single cells with predicted phenotype were collected and lysed in domed caps of 0.2 ml PCR tubes and stored frozen. The lysed cells were spun into PCR tubes with an RT mix, ERCC spike-ins, and reverse transcribed with an RT primer that contained a priming site for amplification (Rev), a random sequence for RNA molecule identification (unique molecular identifier, UMI), a cell barcode (BC) and an Illumina Index Read (IIR). (The template switching oligonucleotide (TSO) adds a second PCR priming site during RT.) After PCR amplification the 3’ biotinylated (*) full-length cDNA was fragmented by tagmentation with EZ-Tn5 transposase (end-joined with mosaic end adaptors, ME) and the 3’ terminal fragments were isolated on

Streptavidin beads. Sequences required for Illumina sequencing (P5, P7) were introduced by PCR prior to sequencing. See methods section for details, primer sequences in Tables S4,5.

**Figure S3: Analysis of gene expression variability in the fate-seq samples.** Related to Figure 2

(**A**) Heatmap of cell cycle scores in each cell, with collection batch and phenotype information associated with each cell displayed on the left panel. No relationship between cell collection, phenotype and cell cycle score was observed.

(**B**) Hierarchical clustering of gene expression levels for the genes identified as most variable in our analysis. The phenotype labels corresponding to each cell are displayed at the top of the graph. The variability in gene expression does not correspond to the phenotype of the cells.

**Figure S4: Molecular functions associated with the differentially expressed genes identified using our fate-seq workflow.** Related to Figure 2

This analysis is based on a subset of genes selected based on nominal p-value < 0.05. Only the most significant molecular functions are represented (-log (p-value) > 1.5). Analyses were generated through the use of IPA (QIAGEN Inc., https://www.qiagenbio-informatics.com/products/ingenuity-pathway-analysis).

**Figure S5: Pharmacological validations of top target gene *DNM1L* using co-treatment with inhibitor drugs.** Related to Figure 2

(**A**) Live-cell microscopy experiments evaluating the effect of Dynasore (20 μM) in combination or not with TRAIL treatment (25 ng/ml) in parental cells expressing IC-RP only. *Violin plots*: maximal caspase-8 activation rate of each cell for each condition of the one representative experiment where 256 cells were tracked. *Survival curves*: cell death times of each condition in the same representative experiment (event determined by morphology assessment in live-cell microscopy). *Bar graphs*: average cell surviving fraction at the end of the live-cell microscopy experiments (10 hr, dead cell counts determined by morphology assessment) for 2 experimental repeats (513 cells were tracked in total), data are represented as mean ± SEM.

FRET ratio trajectories of parental cells expressing IC-RP only treated with TRAIL (25ng/ml) or not (**B**: 155 cells tracked), in combination with Dynasore (20 μM) or not (**C**: 60 cells tracked, and **D**: 132 cells tracked), or in combination with Mdivi-1 (25 μM) or not (**E**: 60 cells tracked , and **F**: 151 cells were tracked) in 10-hours live-cell experiment.

**Figure S6: Live-cell microscopy experiments evaluating the effect of cycloheximide on caspase-8 activation and cell survival upon treatment with TRAIL.** Related to Figure 2

(**A**) Single-cell assessments of caspase-8 activation and cell survival, evaluating the effect of cycloheximide (2.5 μg/ml) in combination or not with TRAIL treatment (25 ng/ml) in parental cells expressing IC-RP only. *Violin plots*: maximal caspase-8 activation rate of each cell for each condition of the one representative experiment where 260 cells were tracked. *Survival curves*: cell death times of each condition in the same representative experiment (event determined by morphology assessment in live-cell microscopy). *Bar graphs*: average cell surviving fraction at the end of the live-cell microscopy experiments (10 hr, dead cell counts determined by morphology assessment) for 2 experimental repeats (440 cells were tracked in total), data are represented as mean ± SEM.

FRET ratio trajectories of parental cells expressing IC-RP only, treated with TRAIL (25 ng/ml) or not (**B**: 168 cells tracked), in combination with cycloheximide (2.5 μg/ml) or not (**C**: 60 cells tracked, and **D**: 134 cells tracked) in 10-hours live-cell experiment.

**Figure S7: Live-cell microscopy experiments evaluating the effect of tin protoporphyrin IX on caspase-8 activation and cell survival upon treatment with TRAIL.** Related to Figure 2

(**A**) Single-cell assessments of caspase-8 activation and cell survival, evaluating the effect of tin protoporphyrin IX (SnPPIX 5 μM, targeting heme oxygenase -HO, encoded by *HMOX1 and 2*) in combination or not with TRAIL treatment (25 ng/ml) in parental cells expressing IC-RP only. *Violin plots*: maximal caspase-8 activation rate of each cell for each condition of the one representative experiment where 263 cells were tracked. *Survival curves*: cell death times of each condition in the same representative experiment (event determined by morphology assessment in live-cell microscopy). *Bar graphs*: average cell surviving fraction at the end of the live-cell microscopy experiments (10 hr, dead cell counts determined by morphology assessment) for 2 experimental repeats (501 cells were tracked in total), data are represented as mean ± SEM.

FRET ratio trajectories of parental cells expressing IC-RP only, treated with TRAIL (25ng/ml) or not (**B**: 148 cells tracked), in combination with tin protoporphyrin IX (SnPPIX 5 μM) or not (**C**: 93 cells tracked, and **D**: 153 cells tracked) in 10-hours live-cell experiment.

**Figure S8: Target genes validation using engineered cell lines: single-cell assessment of caspase-8 activation and cell survival upon treatment with TRAIL.** Related to Figure 2

(**A**) Functional validation of short-listed target genes *UBE2D4*, *UQCC3* (*c11orf83*), *BLOC1S1*, *PRSS56*, and *SLC25A1*, using engineered cell lines: single-cell assessment of caspase-8 activation and cell survival upon treatment with TRAIL (25ng/ml) performed by live-cell microscopy experiments evaluating the effect of overexpressing a target gene in parental HeLa cells expressing IC-RP in each box. Control cells (mRFP1) are IC-RP parentals, overexpressing mRFP1 fluorescent protein only. *Violin plots*: maximal caspase-8 activation rate of each cell for each condition of one representative experiment (number of cells tracked in the experiment shown for *UBE2D4*: 237, *UQCC3*: 239, *BLOC1S1*: 285, *PRSS56*: 270, and *SLC25A1*: 298). *Survival curves*: cell death times of each condition in the same representative experiments shown (event determined by morphology assessment in live-cell microscopy). *Bar graphs*: average cell surviving fraction at the end of the live-cell microscopy experiments (10 hr, dead cell counts determined by morphology assessment in live-cell microscopy) for at 3 experimental repeats (776 total cells tracked for *UBE2D4*, 794 for *UQCC3*, 888 for *BLOC1S1*, 813 for *PRSS56*, and 817 for *SLC25A1*), data are represented as mean ± SEM. *Clonogenic assays*: one representative experiment of at least 3 experimental repeats of crystal-violet stained cells in 96-well plates, one week after a 24h-treatement with TRAIL (250 ng/ml).

(**B**) Quantitative PCR analyses of the target gene expressed in their respective cell lines compared to the IC-RP parental cell line.

(**C**) Functional assessment of *LLPH* gene, performed by live-cell microscopy experiments as described in panel A above. *Violin plots*: maximal caspase-8 activation rate of each cell for each condition of one representative experiment where 373 cells were tracked. *Survival curves*: cell death times of each condition in the same representative experiment (event determined by morphology assessment in live-cell microscopy). *Bar graphs*: average cell surviving fraction at the end of the experiments (10 hr, dead cell counts determined by morphology assessment in live-cell microscopy) for 2 experimental repeats (677 cells were tracked in total), data are represented as mean ± SEM.